

Computer Modelling the Root Cause of Cystic Fibrosis

by

Miro Alexander Astore

*A thesis submitted in fulfilment of the
requirements for the degree of*

Doctor of Philosophy

School of Physics
Faculty of Science
The University of Sydney

2022

Declaration of Original contribution

of the dissertation submitted by

Miro Alexander Astore

This is to certify that to the best of my knowledge, the content of this thesis is my own work. This thesis has not been submitted for any degree or other purposes.

I certify that the intellectual content of this thesis is the product of my own work and that all the assistance received in preparing this thesis and sources have been acknowledged.

Miro Alexander Astore, Author

Date

Abstract

placeholder text

In loving memory of Madeline Jennifer Dell

“Fear cuts deeper than swords.”

Arya Stark

Acknowledgments

Daniel Golestan, a wise man, once told me that to be given the opportunity to create this thesis was a gift. It was. It was a gift given to me by every friend, colleague, teacher, mentor and family member I've spent any time with. The list that follows of those to thank is not complete. If it was you'd be reading about a conversation I had with a middle aged woman in a hostel north of San Francisco, but that has little to do with Cystic Fibrosis.

To My parents raised me with not only academic rigor in mind but also a respect for aesthetics which has served me strangely well. I've never had a talent for the creative side of things compared to quantitative disciplines. But were it not for their demand for respect for the arts I'd have remained illiterate.

To Jeffry for his tutelage and patience, even across the pacific ocean. To have been your first mentee is an honor. You will go far.

To Poker, I am a better human being in every conceivable way for having known you. Your wisdom, intelligence and kindness are boundless. You have taught me an inordinate number of things. And yes, I do mean inordinate.

Nono and Nona I don't think you'll ever read this. I'm sad that you won't understand what I've done but I think you'd be proud if you did. Living in Condell park did more for me than you could know. Far from war torn Beirut or dirt poor Orria I'm sitting in a well lit office writing this with a full stomach and few worries. Sometimes this luck makes my head spin.

Thank you to Shafagh Waters for her vision, her drive and all her advice. You brought me a truly fascinating PhD project and I benefited greatly from your mentorship. Bridging the gap between cell biology and molecular physics is something that will happen more in the future and I'm lucky to have met such a driven lab to teach me to do so.

Serdar, a brilliant mind and a patient boss. Thank you for giving me the best possible experience at grad school I could have asked for. Your willingness to let me pursue self directed projects with a guided hand is a privilege during a PhD and I'm all the better for having gotten it from one of the best. I'm excited to carry some of your physical insight into biological systems to future research projects.

Maddy, I miss you every day. You couldn't have imagined what it was like to do this after losing you. I carry much of you with me and I wish I had more. I miss your intelligence, your warmth and your love.

You're all in my Loop and I hope I'm in yours in some way.

List of Publications

MA - Miro Alexander Astore

SK - Serdar Kuyucak

1. placeholdertext

Publication Authorship Attribution

In addition to the statements above, in cases where I am not the corresponding author of a published item, permission to include the published material has been granted by the corresponding author.

Miro Alexander Astore, Student

Date

As the supervisor for the candidature upon which this thesis is based, I can confirm that the authorship attribution statements above are correct.

Serdar Kuyucak, Supervisor

Date

Contents

List of Abbreviations	ix
List of Figures	xii
List of Tables	xiii
1 Introduction	1
1.1 Physics in a test tube	1
1.2 What is Physics?	2
1.3 Ion Channels: Natures laboratories to Teach Us Biophysics	4
1.4 Studying Cystic Fibrosis to Learn Biophysics	5
1.5 Well. We're in the future	5
2 From Protons to Proteins: Methods to simulate the inside of a cell.	7
2.1 Quantum Mechanics is Not Tractable at the Scale of Biology.	7
2.1.1 A full quantum mechanical treatment	8
2.1.2 The Born-Oppenheimer approximation.	9
2.2 Classical MD, Molecular Motions Without Quantum Mechanics	10
2.2.1 Philosophy of Different Molecular Mechanics forcefields.	14
2.3 Periodic Boundaries to Simulate the Inside of Cell	14
2.4 Controlling the Temperature and Pressure in a Simulation	17
2.4.1 Hot and Cold with the Nosé-Hoover Thermostat	17
2.4.2 Under Pressure with the Parrinello-Rahman Barostat	19
2.5 The Process of Preparing an MD Simulation	20
2.6 Choosing an Appropriate Time Step	20
2.6.1 Verlet Leap-Frog Integration	21
2.7 Free Energy Calculations: Making Simulations More Useful	22
2.7.1 Umbrella Sampling	23
2.7.2 Metadynamics	25
2.8 Short Comings of Classical MD	27
3 Review of the Molecular Cause of Cystic Fibrosis	30
3.1 Clinical outcomes of Cystic Fibrosis	31
3.2 CFTR Structure	32
3.3 CFTR classification and structure	32
3.4 The Gating Cycle	33
3.5 Classes of Misfunction to CFTR	33

3.6	CFTR Modulators	34
3.6.1	Correctors	34
3.6.2	Potentiators	34
3.6.3	Anion Selectivity	35
3.7	Patient Derived Organoids	36
4	Concluding Remarks	37
	References	38
	Bibliography	38

List of Abbreviations

<i>AMBER</i>	Assisted Model Building with Energy Refinement
<i>BAR</i>	Bennett-Acceptance-Ratio
<i>CF</i>	Cystic Fibrosis
<i>CFTR</i>	Cystic Fibrosis Transmembrane Conductance Regulator
<i>CHARMM</i>	Chemistry at Harvard Macromolecular Mechanics
<i>COM</i>	Centre of Mass
<i>CV</i>	Collective Variable
<i>FEP</i>	Free-Energy Perturbation
<i>gA</i>	Gramicidin A Ion Channel
<i>Glt_{Ph}</i>	Glutamate Transporter - <i>Pyrococcus horikoshii</i>
<i>GROMACS</i>	GROningen MACHine for Chemical Simulations - MD program
<i>GROMOS</i>	GROningen MOlecular Simulation - MD program
<i>LJ</i>	Lenard-Jones Potential
<i>MBAR</i>	Multistate Bennett-Acceptance-Ratio
<i>MD</i>	Molecular Dynamics
<i>MetaD</i>	Meta Dynamics
<i>NAMD</i>	Nanoscale Molecular Dynamics - MD Program
<i>NBD</i>	Nucleotide Binding Domain
<i>NPT</i>	Constant number of Particles, Pressure and Temperature
<i>NVT</i>	Constant number of Particles, Volume and Temperature
<i>OpenMM</i>	Open Molecular Mechanics - MD Program
<i>OPLS</i>	Optimised Potentials for Liquid Simulations
<i>PBC</i>	Periodic Boundary Condition
<i>PCA</i>	Principal Component Analysis
<i>PDB</i>	Protein Data Bank
<i>PMF</i>	Potential of Mean Force
<i>PME</i>	Particle Mesh Ewald - Long-range Electrostatics Method
<i>POPC</i>	1-palmitoyl-2-oleoyl-sn-glycero-3-phosphocholine
<i>POPE</i>	1-palmitoyl-2-oleoyl-sn-glycero-3-phosphoethanolamine
<i>RMSD</i>	Root-Mean-Square Deviation
<i>TI</i>	Thermodynamic Integration
<i>TICA</i>	Time-lagged Independent Component Analysis
<i>US</i>	Umbrella Sampling
<i>VMD</i>	Visual Molecular Dynamics - MD Visualisation Program
<i>WHAM</i>	Weighted Histogram Analysis Method

List of Figures

2.1	The Bonded Interactions Calculated In Classical Forcefields	12
2.2	Comparison Between Potentials in Quantum and Classical Forcefields .	13
2.3	The Lennard-Jones Potential	14
2.4	Particle Mesh Ewald Summation	15
2.5	Illustration of Umbrella Sampling	23
2.6	Illustration of Metadynamics	26
3.1	CFTR Structure	31

List of Tables

2.1 Timescales of Motions in a Molecular System	21
---	----

Chapter 1

Introduction

Whatever complexity means, most people agree that biological systems have it. -Frauenfelder and Wolynes??

1.1 Physics in a test tube

Why can't I write down an equation will tell me how long I will live? Or how many hairs I will grow?

This might seem like an inane question but if you asked a physicist for the formula for how long it takes a radioactive material to decay or how long it will take an object to fall into a black hole they will be able to answer easily.

What makes the first set of questions so much more difficult to answer?

I posit that it is the diversity of components that makes biological questions so difficult to ask and answer. Biology distinguishes itself amongst scientific disciplines requiring the study of systems that are both complex and heterogeneous. In the study of more simple physical systems a simple analogy such as a mass on a spring or a gas of hard spheres can be extremely successful in explaining macroscopic phenomena. For biological systems there appears to be too much complexity for such analogies to have the same level of success. They may struggle to answer questions such as "If this gene mutates how will that affect lung function?" "If this drug were given at a higher dosage what would its effect be?" "What if we change this chemical moiety?" At the moment, a trained chemist needs to go and answer these questions pipette in hand, the physicist with their notebook is hopeless.

It seems like a silly question but it seems important to ask why we can't just use a device similar to a harmonic oscillator or a perfect black body to speculate at useful

answers for these quantitative questions. The answer is just as silly. If you look with your naked eye at your arm, you will notice hair, pores, dry skin, dead skin, perhaps even tendons and muscles under the skin. If you take a microscope you will notice the 3 layers to your skin with different functions and composition. If you were to take a single cell from any of those layers and stain it to distinguish features in an electron microscope you would notice all sorts of complex structures and the size and number of these structures would vary depending on where you took the cell from in the body. Within and between each those structures is a salty, wet dance of molecules large and small. This heterogeneity on length scales hints at the reasons behind biology's physical complexity. Plasma physics is often characterised by the density of the plasma studied. This parameter may span 28 orders of magnitude from a dense stellar core to the sparse intergalactic nebulae. The same mathematical tools can be used to map any plasma in these energy scales. Would that we were so lucky in biology. We struggle to apply same physical models to deal with phenomena across a single order of magnitude.

Thus, in order to move towards more predictive theories of biology it is necessary to consider much more of the fundamental physical processes occurring within biological systems than simply searching for statistical trends. One form of this from fundamentals approach is the simulation of every atom in a biological system. Although computationally expensive, this approach appears necessary due to the heterogeneous nature of biological systems.

One of the things we're trying to do with molecular dynamics is fill in the gap left by the sequence- \rightarrow function paradigm which is internalised in current understandings of molecular biology. We usually talk about how the sequence of the gene defines its function because it gives the protein its structure but really there is a considerably larger amount of regulatory pressure exerted by the environment. This is what is missing from the sequence alone paradigm.

1.2 What is Physics?

Personally I have always given answers along the lines of "the study of the movement of energy within a system" or when I was in high school "The study of how things move". Although adequate for a layman these might obscure the fundamental structure within physics that make it such a powerful tool. It is the conception of some causal unit in a system and the ability to scale up the behaviour of that unit to make predictions about measurable phenomena.

This might take a few different forms at different scales, it's what makes physics feel like the most "fundamental" of the sciences.

Examples include:

Newton's laws of gravitation to explain the organisation of the solar system.

Einstein's theories employing Riemannian geometry to track the motions of galaxies and black holes.

The conception of atoms as hard spheres used to derive the macroscopic behaviour of

gasses.

The schrodinger wave function to find the structure of atoms, which can then be integrated further up to find their macroscopic organisations. More on this later.

Biological systems exhibit such a problem for the physicist because unlike the above problems it is extremely hard to pick out a fundamental unit to even begin our upwards journey. An evolutionary biologist might say to choose the "gene" but this is actually far too high in our spatial heirarchy already. Really a gene is only meaningful to the dance of life if it has partners to dance with. Genes of hard spheres ?

A coil of DNA in water doesn't really do much in solution except decay without machinery that can preserve, read, translate and replicate it. The gene is an emergent property, we have to go deeper.

So, what creates the gene?

A slew of biological machinery that mostly take the form of proteins. These proetins are a special case of chemistry, with many observable functions. Their sequence is coded by the DNA in something reminiscent of a strange loop [Hoffstadter2008].

This self referential loop is one of the reasons biology is so difficult. Since we know that this strange loop is kicked off by atomic interactions we will start there. As we are taking a physical, pragmatic approach here it would make sense to begin with the protein, after all, they stave off the march of entropy constantly trying to eat up all of your cells. It also just so happens that they are much easier to understand computationally since their motions are faster and more flexible.

The first level sub cellular organisation is perhaps the most intimidating first step for me personally after spending 4 years simulating a single protein. Glimpsing the complexity within a single one of these molecules has been one of the most existential experiences of my life but the knowledge that there are astronomical numbers of these things inside me all of the time

It is hoped that illustrating the monumental task in both intellectual effort and resources of incrementally increasing the understanding of a single protein amongst tens of thousands will give the reader and understanding of how we might continue our quest to understand the molecular dance that plays within all of us.

This makes sense if we think about it Somewhere on the scale between a single protein and a single cell this is what we consider "life". We have single unicellular organisms but we don't have uniproteomic organisms. So the fundamental length scale of life is somewhere between $10^{-10}m$ and $10^{-3}m$. This is the first loop in our strange loop.

After this things start to run away from me with my handful of GPUs and limited patience. So in this thesis we will only discuss single proteins.

1.3 Ion Channels: Natures laboratories to Teach Us Biophysics

The physiological importance of ion channels became clear after the experiments of Hodgkin and Huxley. These mathematicians took nerves from fished giant squid and measured the current running through the nerve in response to electrical stimulation. What they found was intriguing. Current would only flow when the input signal was of a sufficient voltage. The measurements and modelling they carried out gave an exciting set of results. They found that the cell had to maintain a constant electrochemical gradient, they discovered that the presence of voltage gated ion channels and cation selective ion channels[1]. Each of these features, motivated by mathematical modelling have been found to be critical to the functioning of the cell and fundamental to the foundation of molecular biophysics. The following set coupled ordinary differential equations were discovered by testing functions which fit the measurements taken from the squid axon.

$$\begin{aligned} I &= C_m \frac{dV}{dt} + \bar{g}_K n^4 (V - V_K) + \bar{g}_{Na} m^3 h (V - V_{Na}) + \bar{g}_l (V - V_l), \\ \frac{dn}{dt} &= \alpha_n(V)(1 - n) - \beta_n(V)n, \\ \frac{dm}{dt} &= \alpha_m(V)(1 - m) - \beta_m(V)m, \\ \frac{dh}{dt} &= \alpha_h(V)(1 - h) - \beta_h(V)h \end{aligned} \tag{1.1}$$

The α and β parameters are the proportion of the sodium and potassium channel populations which are activated, respectively. This example shows how basic theoretical tools can be used to predict and discover physical phenomena in biological systems. The Hodgkin Huxley model proved the existence of a cell's resting potential, the possibility of voltage gated ion channels, and channels whose pores are selective for certain ions. Even today the molecular mechanisms behind some of these discoveries are debated. In this thesis we aim to do the same by building up from fundamental quantum mechanics in order to understand the motion of single proteins so we might speculate as to the function of the whole organism.

Similar to the above story, ion channels have always motivated the early pioneers of molecular biophysics. This is due to their ubiquity and importance in biological systems and the ease of measuring their activity with biochemical assays. One just needs an oscilloscope to measure their current. As cell biology has advanced it has become clear that the resting potential of a cell is critical to its function, regulating many chemical reactions inside it.

These factors have allowed biophysicists sufficient data to build sufficiently accurate models of biomolecular systems which generalise to other systems. Leading to a thriving field, analysing systems as diverse as protocells to gold nano particles CITATIONS NEEDED.

The discovery of voltage gated channels and a resting potential .

1.4 Studying Cystic Fibrosis to Learn Biophysics

The sad truth of this debilitating disease is that those afflicted are extremely unlucky. A single, small change to the genome and their lungs fill with sticky mucus and become infected with bacteria, each breath cumbersome. Personally, I've not met somebody who has this disease. I have consistently wondered what perspective I'm missing by not suffering myself from such a condition or even knowing somebody with it. I'm not been trained in the ethics of studying medicine.

In this way, my motivations for studying this protein aren't solely focussed on treating disease. There is a perspective on protein evolution which states that the primary sequence of a particular gene contributes to the overall fitness of an organisms by a formula. []

It just so happens that the CFTR gene sits at the precipice of a daunting cliff in sequence space. So by taking small steps in sequence space and plunging down this cliff we can try to understand how we might push the ball back up the cliff and retain functionality.

Moreover, by learning the nuts and bolts of what goes wrong with CFTR we can start to think about where some of these cliffs might be in other places in the proteome, to gain function and avoid disease and debilitation.

The reality of disease pathogenesis being caused by so many different mutations means that there has been decades of investigation into the function of every domain in the protein.

Due to the array of disease causing mutations which occur accross the cystic fibrosis protein, there is a large body of literature on its unique function. This allows us a glance into its function and an opportunity to simultaneously perform basic biophysical research while directly assisting in furthering patient outcomes.

1.5 Well. We're in the future

Throughout science, the integration of experimental data with theoretical models leads to new and exciting research, this is particularly true in biology with its important applications in medicine, agriculture and manufacturing. Wet lab biologists take advantage of experimental techniques which allow them to understand the dynamics and structure of living things from the top down. The finer the experimental instrument, the finer the detail they may resolve. Conversely, computational and theoretical biologists take a bottom up approach, we aim to take the granular details of a system, and integrate them upwards to model the macroscopic behaviour of that system. With more powerful computers and more detailed models we can make predictions about the behaviour of more complex systems. What is so exciting about the current era of biological research is that the domains of these two approaches are beginning to overlap, where they can synergize and drive further breakthroughs. As we discover more systems where this overlap can be found we will develop more sophisticated treatments for diseases and problems found around the world.

The reason this has happened before in physics is two fold. Physical systems are much more homogeneous. So it's much easier to integrate upwards in length scale. Once you understand the pairwise interaction between two components it's simply a question of having the theoretical and computational capacity to model the bulk behaviour of that system.

The difference with biological systems is that they have so many different components that finding an analytic or even computationally tractable solution is usually impossible. However, as we collect more data and build more powerful computers we can approach more complete models. These in turn inform more powerful theoretical models these help direct the material efforts of experimental expertise .

AlphaFold is a good example. This new breakthrough builds on decades of inquiry from the structural biology community and advancements in AI to give high resolution protein structures. Now this result can be used to fill in the gaps of structural biology. Crucially, AlphaFold knows what it doesn't know. So we can tell where to direct the efforts of structural biology. Together these advances will fill more gaps in our knowledge of protein physics.

Chapter 2

From Protons to Proteins: Methods to simulate the inside of a cell.

This chapter is written for somebody who has studied undergraduate physics and now wishes to model biological systems at the molecular level. Care is taken to dive deeper into the mathematical formulations of simulation methods than is conventionally given in introductory texts. Essentially, this is the understanding of simulation techniques I wish I had when I started studying them. An excellent overview which I would recommend as first reading for any new student can be found in an article by Braun et al. [2] followed by [14] for statistical rigour and [pohorille2010] for free energy calculations.

2.1 Quantum Mechanics is Not Tractable at the Scale of Biology.

Living things are made of atoms and atoms themselves are composed of many particles, protons, neutrons and electrons. The motions these constituent particles are governed by quantum mechanics. Unfortunately, performing simulations for the number of atoms involved in proteins and other cellular components at quantum mechanical accuracy is impossible. Hence, we will show how to take the fundamental formulation of atomic interactions in the Schrödinger wave equation and apply approximations in order to produce a model which is capable of simulating macromolecular systems at biologically relevant timescales.

We will gradually integrate upwards, beginning with the interactions in a single atom we will work our way up to a complex macromolecular system with lipids, water, salts and of course, proteins. Ultimately this section rationalises the treatment of atoms as point charges in classical molecular dynamics simulations.

2.1.1 A full quantum mechanical treatment

Since we are dealing with atoms which are governed by quantum mechanics we must begin our journey upwards with the time dependent form of the Schrödinger wave equation.

$$i\hbar \frac{\partial}{\partial t} \Psi(\mathbf{x}, t) = \left[-\frac{\hbar^2}{2m} \nabla^2 + U(\mathbf{x}, t) \right] \Psi(\mathbf{x}, t) \quad (2.1)$$

In quantum systems we treat all particles as waves hence the use of the wave function $\Psi(\mathbf{x}, t)$. The complex amplitude of the wave function $|\Psi(\mathbf{x}, t)|^2$ tells us the likelihood of detecting the particle at time t and at place \mathbf{x} . The term in the brackets correspond to $-\frac{\hbar^2}{2m} \nabla^2$, the kinetic energy of the particle with mass m while $V(\mathbf{x}, t)$ is an externally applied potential on the system. Given that the left hand term $i\hbar \frac{\partial}{\partial t} \Psi(\mathbf{x}, t)$ contains a gradient with respect to time, it governs how the wave function will evolve in time.

When the external potential V has no explicit dependence on time, this equation reduces to the familiar time independent form.

$$U\Psi(\mathbf{x}, t) = \left[-\frac{\hbar^2}{2m} \nabla^2 + V(\mathbf{x}) \right] \Psi(\mathbf{x}, t) = H\Psi(\mathbf{x}, t) \quad (2.2)$$

Note that the wave function $\Psi(\mathbf{x}, t)$ is still allowed to evolve in time.

In atomic systems there are two types of particles, nuclei which we will denote with the subscript n and electrons denoted by e . In order to treat these elements separately we decompose the Hamiltonian of the system into a few components.

$$H = \underbrace{T_n + U_{n-n}}_{H_n} + \underbrace{T_e + U_{e-e} + U_{n-e}}_{H_e} \quad (2.3)$$

Where T_n and T_e denote the kinetic energy of the nuclei and electrons respectively. While U_{n-n} , U_{n-e} , U_{e-e} denote the potential energy for interactions between nuclei, between electrons and nuclei and between electrons respectively.

Since the potential terms all describe charged species, they follow Coulomb's law and have the form.

$$U_{n-n} = \sum_{i>j} \frac{q_e^2 z_i z_j}{|\mathbf{R}_i - \mathbf{R}_j|}, \quad U_{n-e} = - \sum_{i,l} \frac{q_e^2 z_i}{|\mathbf{r}_l - \mathbf{R}_i|}, \quad U_{e-e} = \sum_{l>k} \frac{q_e^2}{|\mathbf{r}_l - \mathbf{r}_k|} \quad (2.4)$$

Here the z_i represent the atomic number (and thus the charge) of the i th nucleus and q_e is the unit charge of the electron. The reason for the separate coordinates R_i and r_l is to separate out the treatment of nuclei and electrons which will be important once we apply the Born-Oppenheimer approximation.

Meanwhile, the kinetic energy terms are of the form

$$T_n = - \sum_i \frac{\hbar^2}{2M_i} \nabla_i^2, \quad T_e = - \sum_l \frac{\hbar^2}{2m_e} \nabla_l^2 \quad (2.5)$$

M_i represents the mass of the i th nucleon and m_e represents the mass of an electron. The operator $\nabla^2 = \frac{\partial^2}{\partial x^2} + \frac{\partial^2}{\partial y^2} + \frac{\partial^2}{\partial z^2}$. The separate subscripts i and l are due to the different coordinates which we use to denote the positions of the nuclei and the electrons. The reason for this will become clear when we derive the Born-Oppenheimer approximation to separate the wave functions and treat them separately.

2.1.2 The Born-Oppenheimer approximation.

In order to reach the Born-Oppenheimer approximation we start with the observation that electrons have a mass 3-4 orders of magnitude smaller than the nuclei. This motivates two simplifications. The “clamped nuclei assumption” where we solve the Schrödinger equation whilst nuclei are fixed in space and do not move. And a related assumption known as the “adiabatic assumption” which postulates that the electrons will respond instantaneously to any changes in the positions of the nuclei. Combining these physical approximations we derive the “Born-Oppenheimer approximation” for the Schrödinger equation which can be used to simplify calculations involving several atoms at once.

We begin the derivation by examining the time-independent form of the electronic Schrödinger wave equation where the nuclei are fixed at positions R_i .

$$H_e(\mathbf{r}_l, \mathbf{R}_i) \psi_e(\mathbf{r}_l, \mathbf{R}_i) = U_e(\mathbf{R}_i) \psi_e(\mathbf{r}_l, \mathbf{R}_i) \quad (2.6)$$

Fixing the nuclei in this way gives the “clamped nuclei” approximation [3]. To solve the wave function for the whole system Ψ_{tot} we use an *ansatz* which decomposes the wave function with an electronic basis into two components: $(\psi_e)_k$ and $(\psi_n)_k$ which are the k th eigenfunction solutions to H_e and H_n respectively.

$$\Psi_{tot}(\mathbf{r}_l, \mathbf{R}_i, t) = \sum_{k=0}^{\infty} \psi_e(\mathbf{r}_l, \mathbf{R}_i)_k \psi_n(\mathbf{R}_i)_k \quad (2.7)$$

Note that there is an implied direct product between the wave functions $\psi_e(\mathbf{r}_l, \mathbf{R}_i)$ and $\psi_n(\mathbf{R}_i)$. When we substitute this expression into the full Schrödinger equation 2.1 we find the following expression for the k th nuclear eigenfunction [4]

$$i\hbar \frac{\partial}{\partial t} \psi_n(\mathbf{R}_i)_k = \left[- \sum_i \frac{\hbar^2}{2M_i} \nabla_i^2 + U_e(\mathbf{R}_i)_k \right] \psi_n(\mathbf{R}_i)_k + \sum_j C_{kj} \psi_n(\mathbf{R}_i)_j \quad (2.8)$$

Where we have coupled the electronic wave functions to each other with the operator

$$C_{kj} = \int (\psi_e)_k^* \left[\sum_i \frac{\hbar^2}{2M_i} \nabla_i^2 \right] (\psi_e)_j d\mathbf{r} + \frac{1}{M_i} \sum_i \left[\int (\psi_e)_k^* [-\hbar i \nabla_i] (\psi_e)_j d\mathbf{r} \right] [-\hbar i \nabla_i] \quad (2.9)$$

Using the “adiabatic assumption” [4] the off-diagonal terms of C_{kj} can be set to 0. This completely decouples the wavefunction into two components

$$\Psi_{tot}(\mathbf{r}_l, \mathbf{R}_i, t) = \psi_e(\mathbf{r}_l, \mathbf{R}_i)_k \psi_n(\mathbf{R}_i, t)_k \quad (2.10)$$

Since all cross terms from the direct product can be ignored. With the further assumption that the diagonal terms C_{kk} can also be ignored because they are 4 orders of magnitude smaller than the other terms in 2.8 [3].

We now write the Born-Oppenheimer approximated wave equation for an atomic system.

$$i\hbar \frac{\partial}{\partial t} \psi_n(\mathbf{R}_i)_k = \left[- \sum_i \frac{\hbar^2}{2M_i} \nabla_i^2 + U_e(\mathbf{R}_i)_k \right] \psi_n(\mathbf{R}_i)_k \quad (2.11)$$

By rearranging this equation and taking derivative we can see how to use Newton’s equations of motion to calculate the forces on the nuclei from the surrounding electric potential

$$M_i \ddot{\mathbf{R}}_i(t) = -\nabla_i U_e(\mathbf{R}_i) \quad (2.12)$$

By choosing an appropriate time-step one can simply iteratively solve this equation of motion to understand the dynamics of an atomic system. The nuclei will move according to their relative positions to each other and the electron clouds will rearrange in response to that motion. There is no need to calculate the interactions between the nuclei and the electrons. This is sufficient accuracy to simulate many physical phenomena with the notable exception of energetic, fast interactions between nuclei and electrons such as spectroscopic phenomenon [3].

2.2 Classical MD, Molecular Motions Without Quantum Mechanics

The Born-Oppenheimer approximation gives rise to Hartree-Fock methods and density functional theory (DFT). These more sophisticated physical methods allow us to simulate the organisation of electron clouds around small molecules, finding broad applications in chemistry and materials science [5]. We can derive the energy profile of certain degrees of freedom within the molecule such as the energetics of stretching out a bond or twisting a dihedral angle. These can be useful when designing novel materials.

However, even with these approximations simulating a large number of atoms is still not computationally tractable. State of the art DFT methods can only simulate up to a few 10s of thousands of atoms [6] and scales as $O(N^3)$ [7]. This is not sufficient to simulate proteins and their surrounding solvation environment. So, we must use another round of approximations to reach the spatial and time scales necessary to simulate biological molecules. We do this by creating a set of mathematical functions the calculations further. Here we use a set of virtual springs and other simple models for the energetic interactions between atoms. This creates what's known as an effective potential.

This formulation gives us classical molecular dynamics sometimes referred to as molecular mechanics. The aim of the classical forcefields discussed here is to use *ab initio* MD as a target to approximate.

The CHARMM effective potential employed in this work is similar to those found in all common all-atom molecular dynamics forcefields. The same functional forms are used in other forcefields such as AMBER, GROMOS and OPLS but with different parameters and design philosophies[9].

We split up the molecular potential into several components dealing with the energies from covalent bonds, including bond stretching, twisting and bending. As well as energies associated with the forces that atoms exert on each other when they are not bonded together. Namely Coulomb forces due to electric charges on the atom and attractive Van Der Walls interactions and repulsion due to Pauli Exclusion the latter two forces are combined into one term we will analyse in detail U_{LJ} .

$$U_{MM} = \underbrace{U_{LJ} + U_{Coulomb}}_{U_{non-bonded}} + \underbrace{U_{bonds} + U_{angles} + U_{dihedrals} + U_{impropers}}_{U_{bonded}} \quad (2.13)$$

Interestingly, the bonded terms may all reasonably be approximated by harmonic springs

$$\begin{aligned} U_{bonded} = & \sum_{bonds} k_b(b - b_0)^2 + \sum_{angles} k_\theta(\theta - \theta_0)^2 + \sum_{Urey-Bradley} k_u(r_{UB} - r_{UB_0})^2 \\ & + \sum_{dihedrals} k_\varphi(1 + \cos(n\varphi - \delta)) + \sum_{improper-dihedrals} k_\phi(\phi - \phi_0)^2 \end{aligned} \quad (2.14)$$

Here, the k_i terms correspond to the strength of the harmonic restraint for that parameter. The 0 subscript denotes the equilibrium position for that parameter. Even though this formulation is quite simple, it has empirically been shown to be a reasonable approximation for the potential energy functions of quantum mechanics in covalently bonded bonded species. Examples can be seen in figure 2.2.

In classical forcefields the non-bonded interactions are expressed using the Couloumb's law because the partial charges assigned to each atom and the Lennard-Jones potential to approximate the interactions arising from both Pauli exclusion and Van Der Walls Interactions.

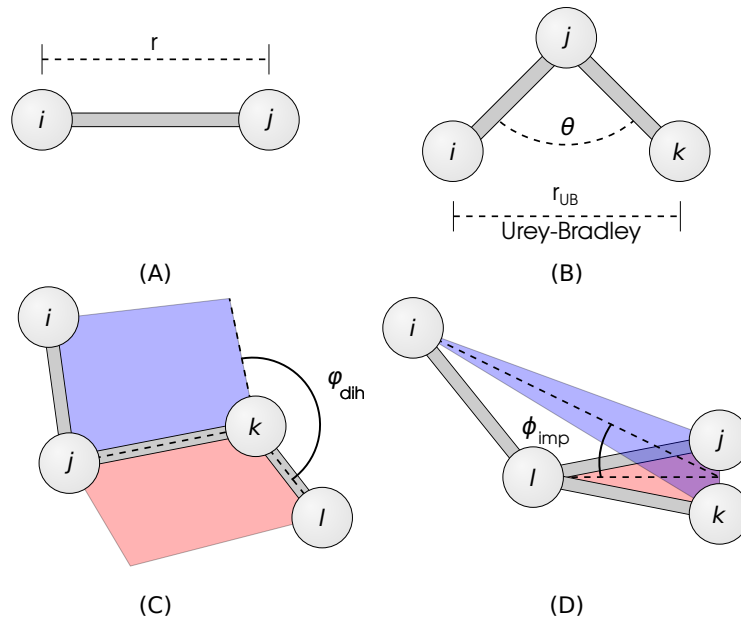


Figure 2.1: The Bonded Interactions Calculated In Classical Forcefields.

(A) The energy of Bond Stretching is approximated as a harmonic oscillator with respect to their separation r . (B) Angles between neighbouring covalently bonded atoms are also approximated as a harmonic oscillator with respect to the angle θ . In some forcefields such as CHARMM there is a correction term for these angular interactions known as Urey Bradley forces. This is calculated using the separation between the non-bonded atoms $i-k$ in the triplet with the parameter r_{UB} . (C) The dihedral angle between four atoms is calculated by constructing two planes. Each plane is constructed to contain three of the four atoms in the set. One plane encompasses atoms i, j and k here colored in blue and the other plane contains the j, k and l atoms colored in red. The dihedral angle is then calculated by taking the angle between these two planes along the line they intersect, the line formed by the $j-k$ bond. (D) The improper dihedral angles enforce the planarity of a molecular configuration. A plane is constructed to contain the i, j and k (blue) atoms and another plane is constructed to contain the j, k and l atoms (red). The improper angle is then calculated as the angle between these two planes.

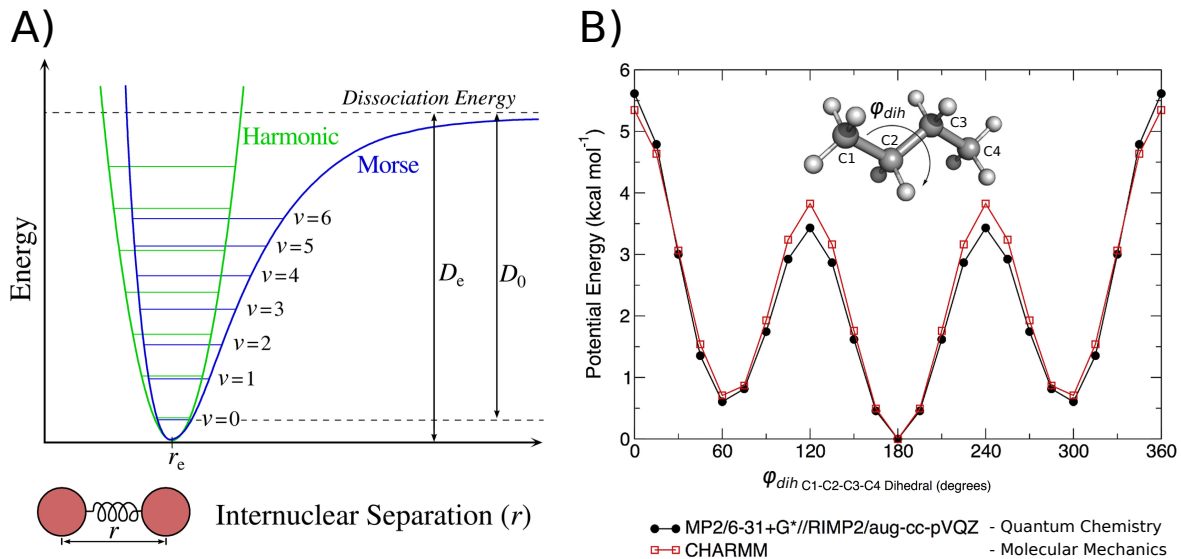


Figure 2.2: Comparison Between Potentials in Quantum and Classical Forcefields

A) The Morse potential was formulated to approximate the potential the potential energy surface associated with the stretching of covalent bonds (blue). At low temperatures (the ground state, $v = 0$) like those found in classical MD there is good agreement between the Morse potential and the harmonic oscillator (green). Credit Mark Somoza 2006 B) Here the potential of the dihedral angle between the atoms C1,C2,C3 and C4 in a butane molecule is calculated using two methods: Quantum Chemical calculations and approximations using the functional form in 2.14 [9]. Note how the appropriate choice of k_φ , n and δ have closely approximated the results the more accurate quantum mechanical calculations.

$$U_{non-bonded} = \underbrace{\sum_{i>j} \epsilon_{ij} \left(\left(\frac{\sigma_{ij}}{r_{ij}} \right)^{12} - \left(\frac{\sigma_{ij}}{r_{ij}} \right)^6 \right)}_{U_{Lennard-Jones}} - \underbrace{\sum_{i>j} \frac{q_i q_j}{r_{ij}}}_{U_{coulomb}} \quad (2.15)$$

The σ parameter denotes the location of the local minima in the Lennard-Jones potential. This is the optimum distance that two atoms will rest against each other in the absence of other effects. The ϵ parameter denotes the depth of the potential well, or how stable the two atoms will be in the minimum energy configuration. This is very important for certain physical parameters such as osmotic pressure [8]

Conversely, the partial charges in a system have the greatest influence on the solvation energy.

By focussing on these two physical parameters we can isolate and improve the non-bonded parameters.

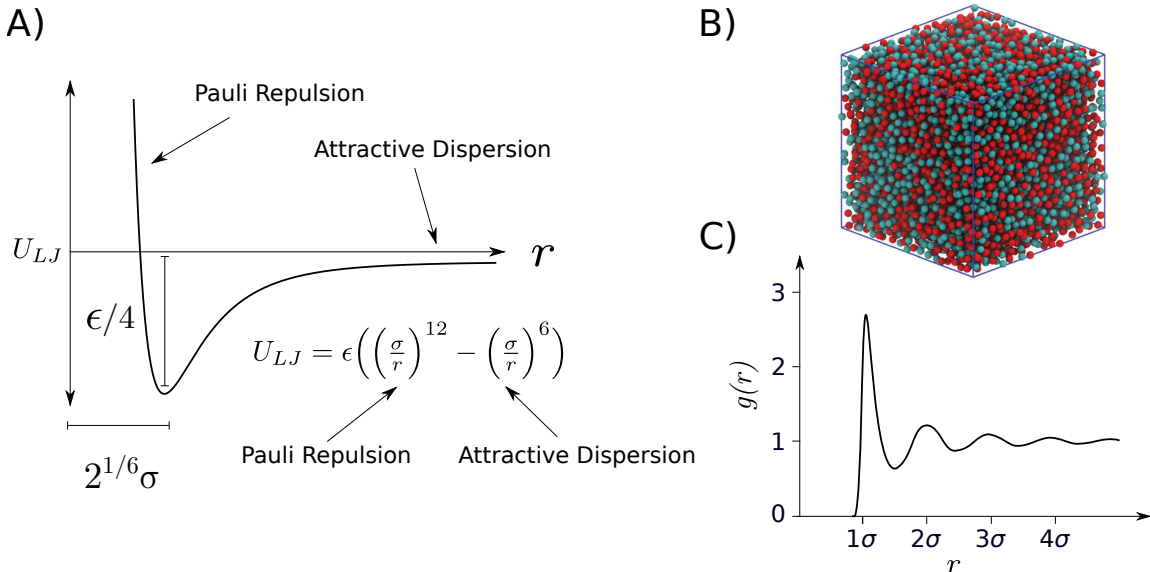


Figure 2.3: The Lennard-Jones Potential

A) The Lennard-Jones potential function has two regimes, the far region one dominated by attractive dispersion forces and the close region dominated by repulsion. In the case of atomic systems this is due to the Pauli exclusion principle. B) An example of a fluid modelled with Lennard-Jones particles [10]. C) The radial distribution function (g) for a Lennard-Jones fluid [11]. Note that the peaks in the distribution are roughly 1σ apart.

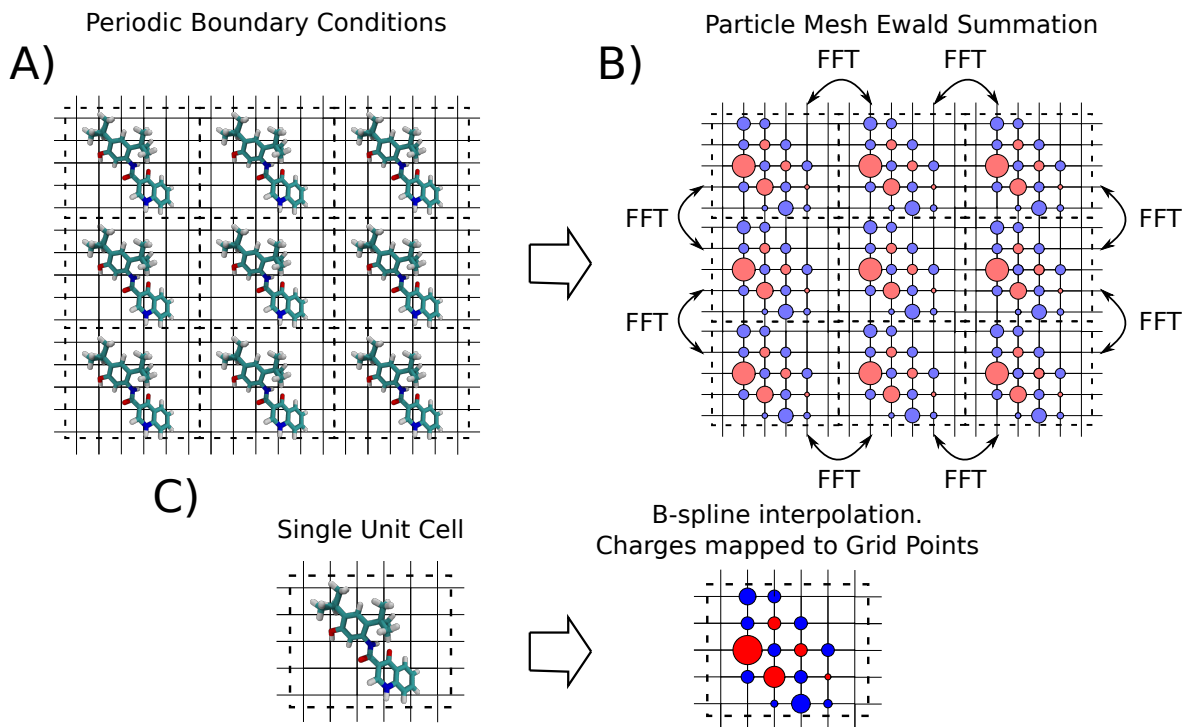
The Lennard-Jones Potential

2.2.1 Philosophy of Different Molecular Mechanics forcefields.

At the time of writing, the four popular forcefields for the simulation of biomolecules are: AMBER, CHARMM, GROMOS and OPLS. Each of these have a slightly different philosophy in their formulation. They may be bottom up, as in the case of AMBER and CHARMM or top down, in the case of GROMOS and OPLS. Bottom up forcefields take the results from quantum *ab initio* calculations and approximate them with the functional form mentioned above. Conversely, top down forcefields take experimental measurable such as Osmotic pressure, solvation energy. This philosophy is closest to physics

2.3 Periodic Boundaries to Simulate the Inside of Cell

Inside cells, proteins are immersed in a large solvation environment composed of water and salts [12]. In order to avoid artefacts we have to replicate this environment somehow[13]. We could make a simulation box large enough to replicate the behavior of a bulk solvent, but even with a large simulation box we can still observe artifacts associated with the vacuum at the boundaries [14]. So, to avoid these boundary effects we use periodic boundary conditions (PBCs), allowing atoms to move between

**Figure 2.4: Particle Mesh Ewald Summation**

A) The molecular system is repeated infinitely along all axes, when atoms reach the edge of the simulation box they are allowed wrap around to the other side of the box. B) The charges in the infinite periodic system are approximated as Gaussian functions on a grid. Then the potential on these screening charges is calculated via a Fast Fourier Transform (FFT). C) A more detailed view of the charge mapping procedure. The point charges in the system are interpolated onto the grid using B-spline interpolation.

images in the simulation box 2.4. This replicates the molecular system infinitely in every direction.

Using PBCs might remove vacuum from our molecular system but now we have a different problem. Effectively, with the PBCs, we have created a system with an infinite number of atoms. We have to somehow limit the number of computations we perform. We could simply truncate the calculation of interactions $U_{\text{non-bonded}}$ after a certain cutoff distance. This is not an issue for U_{LJ} because the $1/r^6$ and $1/r^{12}$ terms in 2.3 decay very quickly for large r . Inaccuracies due to this approximation can be further ameliorated with the use of a smooth switching function [15][16]. On the other hand, the $1/r$ dependence in U_{coulomb} scales much more slowly so truncating it leads to many artefacts in the simulation.[17][18][19][20][21]. Note that this periodicity requires that the unit cell is neutral, else the contribution of potential energy from U_{coulomb} will be infinite, leading to artifacts [22].

To avoid these artefacts and limit computational intensively of our calculations we use a clever scheme known as Particle Mesh Ewald Summation. Interestingly, this scheme ends up scaling better than the pairwise summation in equation 2.15 might imply. The direct summation scales with computational complexity of $O(N^2)$ with the number of atoms while the infinite PME scheme scales as $O(N \log N)$ [23], though there are some further considerations for large systems on parallel architectures [24]. Even with these sophisticated algorithms, the calculation of electrostatic potential still represents the largest computational bottle-neck in classical MD [24].

For a detailed review of different Particle Mesh Ewald Summation methods and the mathematics behind the method see [25]. A brief outline of the Smooth Particle Mesh Ewald summation is given below

1. Point charges from atoms are interpolated onto a grid using B-spline interpolation functions. This procedure is demonstrated in figure 2.4.
2. The charge density functions in the grid are transformed into k -space using Fast Fourier Transforms.
3. The Poisson equation is solved numerically in k -space.

$$\nabla^2 \tilde{U} = \tilde{\rho}(\mathbf{k}) \quad (2.16)$$

Where \tilde{U} is the component of U_{coulomb} we solve for in k -space and $\tilde{\rho}$ is the fourier transform of the smooth scalar function for the interpolated charge densities.

4. An inverse Fourier transform is calculated to calculate solution to the Poisson equation in real space.
5. Now that U_{coulomb} is known at every position in the unit cell we can move atoms according to this potential using Newton's second law.

2.4 Controlling the Temperature and Pressure in a Simulation

Living things are very sensitive to their external environment. Enzymes only work in a narrow range of temperatures and cells burst apart in the absence of pressure. As such, to correctly understand the events in biological bodies with simulations we not only need to correctly calculate the forces being exerted on every atom in their bodies but we must also make sure that the virtual environment in our simulations matches that found in the body or in the laboratory. Conceptually, we seek to approximate the environment as an open topped test-tube sitting in a pressure and temperature controlled laboratory. To do this, we make use of some statistical ensembles chosen for their performance in regulating the thermodynamic quantities in a simulation and their computational expense.

2.4.1 Hot and Cold with the Nosé-Hoover Thermostat

Remember that the temperature of a system is a direct function of the velocity of its constituent atoms. So by regulating the ensemble of velocities we can control the temperature. We begin by choosing the velocities of the atoms within the system from a Maxwell-Boltzmann distribution.

$$f(v_i) = \left(\frac{m_i}{2\pi k_B T} \right)^{3/2} \exp \left(- \frac{m_i v_i^2}{2k_B T} \right) \quad (2.17)$$

Where $f(v_i)$ is the proportion of particles with velocity v_i , k_B is Boltzman's constant. Note that $i = 1, \dots, N_{df}$ as we choose a velocity component for x, y and z components separately.

Despite starting from the same Cartesian coordinates, randomly sampling velocities from the Maxwell-Boltzmann means that replicate simulations will immediately begin from different points in phase space. They will quickly diverge, raising questions around how long one should run a simulation and how many replicates they should run in order to collect reliable statistics. According to Knapp et al.[26], a good rule of thumb is to simulate between 5 and 10 replicates depending on the availability of computing resources. Due to the availability of computer time and the requirement to simulate long time scales to capture the slow motions in CFTR. In this thesis simulations were run in 3 replicates with runtimes between 1 and 2 microseconds.

After the initial choice of velocities, the temperature in a simulation is maintained by directly modulating the velocities of the atoms to maintain the target temperature T_0 . There are many schemes which attempt this. We will discuss the Nosé-Hoover thermostat in detail because it was widely used during the production runs in this thesis. However, for the equilibration phase of the simulation we used the Berendsen thermostat because it is faster at correcting large temperature differentials but does not produce the correct statistical ensemble [27]. We also note that the field has since moved on to favor the Bussi thermostat which is an extension of the Berendsen thermostat which as it works well in most contexts [27][2].

The Nosé-Hoover thermostat is characterised by the use of an extra massive particle coupled to an external bath. This particle is in turn baths to a chain of baths [28][29]. The use of a single bath has been associated with issues with ergodicity and so usually this particle is coupled to a chain of external baths. The Hamiltonian for the Molecular Dynamics System Coupled to a chain of M external baths is then

$$H_{NH}(\mathbf{x}, \mathbf{p}, \eta_1, \dots, \eta_M, p_{\eta_1}, \dots, p_{\eta_M}) = H_{MM} + \sum_j^M \frac{p_{\eta_j}^2}{2Q_j} + k_B T N_{df} \eta_1 + k_B T \sum_{j=2}^M \eta_j \quad (2.18)$$

Here, usually $N_{df} := 3N$ unless there are constraints placed within the system to freeze atoms. η denotes the coordinates in the thermostat of freedom for the thermostat (a scalar variable) with mass Q and H_{MM} is the Hamiltonian defined by

$$H_{MM}(\mathbf{x}, \mathbf{p}) = \underbrace{\sum_i^N \frac{\mathbf{p}_i^2}{2m_i}}_{E_{kinetic}} + U_{MM}(\mathbf{x}). \quad (2.19)$$

By using Hamilton's equations of motion, H_{NH} evolves by

$$\begin{aligned} \dot{\mathbf{x}}_i &= \mathbf{p}_i/m_i \\ \dot{\mathbf{p}}_i &= \mathbf{F}_i - \mathbf{p}_i \frac{p_{\eta_1}}{Q_1} \\ \dot{\eta}_j &= p_{\eta_j}/Q_j \\ \dot{p}_{\eta_1} &= \left[\sum_i^N \frac{\mathbf{p}_i^2}{m_i} - N_{df} k_B T \right] - p_{\eta_1} \frac{p_{\eta_2}}{Q_2} \\ \dot{p}_{\eta_j} &= \left[\frac{p_{\eta_{j-1}}^2}{Q_{j-1}} - k_b T \right] - p_{\eta_j} \frac{p_{\eta_{j+1}}}{Q_{j+1}} \\ \dot{p}_{\eta_M} &= \left[\frac{p_{\eta_{M-1}}^2}{Q_{M-1}} - k_b T \right] \end{aligned} \quad (2.20)$$

Where \mathbf{F}_i is the force vector on the i th particle. It may be calculated from U_{MM} using equation Newton's second law.

The parameters Q_j are chosen by the user to control the coupling strength of th baths to each other. We usually choose

$$Q_j = \frac{\tau_{NH} T}{4\pi^2} \quad \forall j \quad (2.21)$$

where τ_{NH} is the time interval between when the thermostat parameters are updated. This means that whenever the simulation is not at a timestep that is a multiple of τ_T we can just evaluate U_{MM} as normal but every interval of τ_{NH} we rescale the velocities according to the equations of motion in ?? to match the correct temperature T .

Remember that we can always calculate the temperature kinetic energy using the following

$$E_{kinetic} = \frac{3}{2} N k_B T \quad (2.22)$$

2.4.2 Under Pressure with the Parrinello-Rahman Barostat

Pressure is critical to the function of living organisms. Membranes burst apart at low pressures[30] and at high pressures cellular function is disrupted[31]. In order to accurately reflect the atmospheric pressure at which living things thrive we have to accurately calculate and modulate it during our simulation.

In order to measure the pressure at the simulation walls we follow the procedure in [32]. We begin by calculating a quantity known as the virial:

$$W(\mathbf{x}) = \sum_i^{N-1} \sum_{j>i}^N \mathbf{r}_{ij} \cdot \mathbf{F}_{ij} \quad (2.23)$$

where $\mathbf{r}_{ij} = \mathbf{x}_i - \mathbf{x}_j$ is the Cartesian distance between the i th and j th atoms, while \mathbf{F}_{ij} is the force extorted on atom j by atom i .

This is then substituted into the equation

$$P(\mathbf{x}) = \frac{Nk_B T + \langle W \rangle_i}{V} \quad (2.24)$$

And so using equation 2.24 we can see how we can modulate the volume V of the simulation in order to control the pressure throughout the simulation.

To modulate the pressure we apply the Parrinello-Rahman barostat [33][34], with a procedure with a similar philosophy to the extended Hamiltonian used in the Nosé-Hoover thermostat. In this way the system is coupled to an external pressure bath rather than an external temperature bath. First we define that the basis vectors for the periodic simulation box to be $\underline{h} := [\mathbf{a}, \mathbf{b}, \mathbf{c}]$. When the box is scaled to change the volume these basis vectors are multiplied by a set of scalars $s_i := (\xi_i, \eta_i, \zeta_i) \in [0, 1]$. We perform a change of coordinates so that the contributions of the particles onto the boundaries is easily calculated from our equations so we express the atomic coordinates as

$$\begin{aligned} \mathbf{x}_i &= \xi_i \mathbf{a} + \eta_i \mathbf{b} + \zeta_i \mathbf{c} \\ &= \underline{h} \mathbf{s}_i \end{aligned} \quad (2.25)$$

Define $\underline{G} := \underline{h}^T \underline{h}$. The Lagrangian for the scaling system then becomes

$$L = \frac{1}{2} \sum_i^N m_i \dot{\mathbf{s}}_i^T \underline{G} \dot{\mathbf{s}}_i - \sum_i \sum_{j>i} \phi(\mathbf{r}_{ij}) + \frac{1}{2} M \text{Tr}(\underline{h}^T \underline{h}) - P_{ext} V \quad (2.26)$$

Here, M is a constant of proportionality associated with the kinetic energy derived from the movement the particles undergo as they scale. It has units of mass. P_{ext} is our target, externally applied pressure and ϕ represents the pairwise potential from U_{MM} between the i th and j th atoms. This Lagrangian allows us to derive the equations of motion

$$\begin{aligned}\ddot{\mathbf{s}}_i &= - \sum_{j \neq i} \frac{1}{m_i \mathbf{r}_{ij}} \frac{d\phi(\mathbf{r}_{ij})}{dr_{ij}} (\mathbf{s}_i - \mathbf{s}_j) - G^{-1} \dot{G} \dot{\mathbf{s}}_i \\ \ddot{\mathbf{h}} &= \frac{1}{M} (\mathbf{Y} - P_{ext}) \underline{\sigma}\end{aligned}\tag{2.27}$$

The matrix $\underline{\sigma} := V(\mathbf{h}^T)^{-1} = V[\mathbf{b} \times \mathbf{c}, \mathbf{c} \times \mathbf{a}, \mathbf{a} \times \mathbf{b}]$ contains information about the size and orientation of the simulation box, while

$$\mathbf{Y} = \frac{1}{V} \sum_i m_i (\underline{h} \dot{\mathbf{s}}_i) (\underline{h} \dot{\mathbf{s}}_i)^T + \sum_i \sum_{j > i} \frac{1}{r_{ij}} \frac{d\phi(\mathbf{r}_{ij})}{dr_{ij}} \mathbf{r}_{ij} \mathbf{r}_{ij}^T\tag{2.28}$$

represents is the stress tensor which acts accross each of the faces of the unit cell.

This system of equations can be solved numerically to control the pressure of the simulation system by modulating the length of the basis vectors a, b and c contained in \underline{h} .

2.5 The Process of Preparing an MD Simulation

The process of taking a molecular structure and putting it in a cellular environment to simulate it at physiological temperatures is both an art and a science. It's a science because a biophysicist must be aware of the many tricks that structural biologists use to image a macromolecular complex. But it's an art because accounting for those tricks and modifications is rarely straight forward. How do you build a missing loop? What charge state is an amino acid most likely to take during the physiological context.

2.6 Choosing an Appropriate Time Step

The discrete time step, Δt in equation ??, is one of the most important determinants in the performance of the simulation. We would like Δt to be as large as possible, so that the minimum number of calculations are made to sample the desired time scale. In the case of proteins this usually runs between 10^{-6} and 10^{-3} s[36].

Due to Nyquist's theorem the largest Δt parameter we can choose *must* be less than half the speed of the fastest degree of freedom in the system [37]. However, empirically we have found that condensed matter systems require even shorter time steps to maintain their stability [38]. The Verlet leap-frog scheme used in most MD codes requires 5 integration steps per period of the fastest harmonic oscillation in a system [39][40]. The choice of too large a timestep means that the system will escape local free energy minima, accumulating kinetic energy and eventually "blow-up" [2]. In the case of

Motion	Timescale
Covalent Bond-stretching	$1 - 2 \times 10^{-15}$ s
Covalent Bond-angle bending	$5 - 10 \times 10^{-15}$ s
Sidechain Motions	$10^{-12} - 10^{-6}$ s
Rigid Body Motions	$10^{-9} - 1$ s
Ion Conduction	$10^{-9} - 10^{-6}$ s
Protein Conformational Changes	$10^{-9} - 10^{-3}$ s
Alpha Helix Formation	$10^{-9} - 10^{-6}$ s
Beta Sheet Formation	$10^{-6} - 10^{-3}$ s
Protein Folding	$10^{-6} - 10$ s

Table 2.1: Timescales of Motions in a Molecular System

The time step of a simulation must be small enough to capture the motions in the fastest degree of freedom. In hydrogen-rich biomolecular systems the bottle neck can be found in the fast bond vibrations in lighter atoms. This stands in tension with the phenomena we are interested in on longer timescales such as protein folding. Sources: [38][44][45][46][47] [40]

biomolecular systems we are challenged by the fact that they are so hydrogen-rich. Since hydrogen is so light, its motion is much faster compared to the other molecular motions involving heavier, slower moving atoms. Its correlation time is on the order of 1 femtosecond, in classical simulations we are able to get away with using 2 femtoseconds with the use of specialised integration schemes such as SHAKE[41] and LINCS[42] to constrain the fast motion of hydrogen atoms. Allowing us to use $\Delta t = 2\text{fs}$ in during atomistic classical MD simulations.

The use of schemes such as hydrogen mass repartitioning [43], virtual site topologies [40] and multiple time step schemes[streett1978] have also gained popularity in recent years in order to increase time steps further, to $\Delta t = 5\text{fs}$.

As you can see in table ?? the fastest motion in molecular systems is dictated by the translation of hydrogen atoms. Virtual site topologies aim to remove the requirement for calculating these motions every time step by instead interpolating the positions of hydrogen atoms from the positions of surrounding heavy atoms. This follows from the 3600cm^{-1} peak in the resonance infrared resonance spectrum of biomolecules corresponding to the bond stretching oscillation of the H-O bond. [44] Setting the time step of simulations to 1/10th of this period gives sufficient gives the Verlet integrator sufficient resolution to capture the motion and maintain the stability of the energy function.

2.6.1 Verlet Leap-Frog Integration

To produce molecular trajectories we can use the potential U_{MM} which we calculated with equation 2.13 and calculate the forces exerted on the atoms in the system. By Newton's 2nd law we have

$$\mathbf{a}(\mathbf{x})_i = \frac{d^2\mathbf{x}_i(t)}{dt^2} = -\frac{1}{M_i}\nabla_i U_{MM}(\mathbf{x}_i). \quad (2.29)$$

We can use this calculation of acceleration a_i of the i th atom to update the positions and velocities of the atoms in the molecular system with the following triplet of equations known as the leap-frog verlet method [44]:

$$\begin{aligned}\mathbf{v}_i^{n+1/2} &= \mathbf{v}_i^{n-1/2} + \Delta t \mathbf{a}_i^n \\ \mathbf{x}_i^{n+1} &= \mathbf{x}_i^n + \Delta t \mathbf{v}_i^{n+1/2} \\ \mathbf{v}_i^{n+1} &= \mathbf{v}_i^{n+1/2} + \frac{\Delta t}{2} \mathbf{a}_i^{n+1}\end{aligned}\tag{2.30}$$

Note that $v_i^{n-1/2}$ will have been calculated during the previous time step and a_i^{n+1} may be calculated by the updated positions found by calculating \mathbf{x}_i^{n+1} .

In MD, we are less concerned with the accuracy of a particular trajectory so much as collecting sufficient statistics to calculate macroscopic properties such as free energies or diffusion profiles. This means the choice 4th order solvers such as the Runge Kutta method would be inappropriate. Although they may use a large timestep they require 4 evaluations of U_{MM} per timestep and are thus expensive. Hence, we prefer symplectic (energy preserving), 2nd order methods such as verlet integration so the simulation remains stable after millions of timesteps[streett1978].

2.7 Free Energy Calculations: Making Simulations More Useful

The above work sets out how to perform what is known as unbiased MD simulations. These are powerful tools but as will be discussed in section ?? if one only relies on unbiased simulations they will quickly exceed the available computer power. Imagine there is an event our system undergoes that we know from experimental evidence our system must exist but is slow. Examples of this include the passage of an ion through a channel and the binding of a drug. We *could* calculate the Gibbs free energy of a given molecular configuration \mathbf{x}_0 using

$$G(\mathbf{x}_0) = -\frac{1}{k_B T} \ln(P_u(\mathbf{x}_0)).\tag{2.31}$$

Where $P^u(\mathbf{x}_0)$ represents the probability of obtaining state \mathbf{x}_0 , estimated from an unbiased simulation. From here on a subscript of u indicates a quantity obtained from an unbiased simulation and a subscript b represents a quantity from a biased simulation.

Equation ?? shows how there is exponentially poor sampling in regions with high U_{MM} . So it is clear that we will not collect sufficient statistics for a good estimate with available computer power. So, we must be clever in how we direct our available resources. This means intelligently sampling sections of the molecular phase space which are of interest to us physically, but are not reached in our unbiased simulations. A technique that is used extensively throughout this thesis is the addition of a biased potential to the molecular potential U_{MM} calculated for the purposes of unbiased simulations. This will drive the simulation to regions of interest.

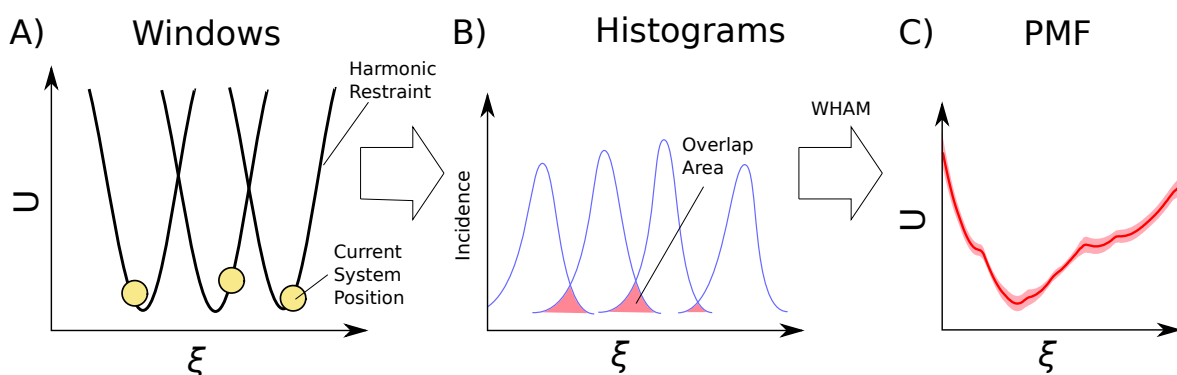


Figure 2.5: Illustration of Umbrella Sampling

A) Several simulations are repeated with only one change. A bias potential is added somewhere along the reaction coordinate ξ . B) The value of ξ is recorded in each of the windows and then graphed as histograms. C) The Overlap in neighbouring histograms is integrated via the WHAM method to calculate the Potential of Mean Force. This gives us the energy landscape. Fluctuations in the overlap in the data can be used to estimate the error for the PMF.

$$U'_{MM} = U_{MM} + U_{bias}(\xi) \quad (2.32)$$

Note how the U_{biased} term is explicitly dependent on a parameter ξ . This parameter is known by many names, an order parameter, a collective variable or a reaction coordinate. Each of these names has its origin in a different subfield but they all refer to the progress toward a target state. This could be a phase transition from a liquid to a gas, the progress of a chemical reaction or more likely in our case, the distance toward a target molecular configuration.

The functional form of U_{bias} depends on the Free energy technique being employed. There are two varieties of techniques, equilibrium and non-equilibrium methods. We will focus on the equilibrium methods in this work. We note that there is another set of methods called alchemical methods which modify the chemical composition of the system which we will not cover.

2.7.1 Umbrella Sampling

This is possibly the most popular method of calculating the potential of a system along a reaction coordinate. The conceptual philosophy for the method is demonstrated in figure 2.6. The molecular system is replicated in several "windows" and a harmonic U_{biased} is added at several points along the collective variable ξ . Statistics are then collected in order to calculate the potential of mean force (PMF) and thus the energy landscape along between those windows.

The functional form of U_{bias} in umbrella sampling is then separated into N windows. With the n th window having the biasing function:

$$U_b^n = \frac{k_\xi^n}{2}(\xi(\mathbf{x}) - \xi_0^n)^2 \quad (2.33)$$

Where ξ_0^n is the equilibrium position of the restraint. k_ξ^n is the strength of the harmonic restraint in the n th window. Typically this is the same in all windows. The more overlap between adjacent windows the more those windows are attracted to each other and the steeper the gradient of the free energy surface (FES) must be pushing those windows together. Conversely, when there is less overlap between adjacent windows it indicates the presence of a barrier in the energy landscape between those windows.

Umbrella sampling is extremely useful for calculating all sorts of experimental quantities and physiologically relevant properties such as folding energies [48], lipid binding [49], ion conduction [50], and drug binding [51]. However, it is particularly sensitive to the choice of initial configuration and collective variable [49]. The former issue is particular to umbrella sampling because generally short runs are used since so many windows are spawned during the method, the simulations must be at equilibrium *before* the method is attempted, and then sufficient statistics must be collected to average over any conformational changes orthogonal to the collective variable. In these ways, care must be taken when using this method to not introduce systematic error into the calculation [52]. A deep knowledge of the molecular system under investigation can help alleviate some of these issues.

Weighted Histogram Average Method (WHAM)

There are a few candidates for calculating the PMF using the statistics calculated in umbrella sampling. The Weighted Histogram Average Method (WHAM)[**kumar1992**], Umbrella Integration (UI)[**kastner2005**] and the Multistate Bennet Acceptance Ratio (MBAR)[**kim2012**] are all used. We will briefly outline the mathematical formulation and estimation of errors of the WHAM method as it is more popular[**53**]. Our explanation follows [54] which covers the topic in more detail.

The method begins by dividing the sampled region into a set of K histograms with K being greater than the number of biased windows N . The whole PMF can be estimated (poorly) from the j th biased histogram using

$$P_u^j(\xi) = P_b^j(\xi) \exp(\beta U_b^j(\xi)) \langle \exp(-\beta U_b^j(\xi)) \rangle \quad (2.34)$$

Where the $P(\xi)$ functions represent the probability density function calculated from samples collected at point ξ . The samples collected in each of these regions gives us an estimate of the PMF in the region according to equation ???. These estimates are combined in a weighted sum using

$$P_u(\xi) = \sum_j^K p_j(\xi) P_u^j(\xi) \quad (2.35)$$

where the weights, $\sum_j^K p_j = 1$ are chosen such that the statistical error is minimised. This means an optimisation problem for the variance of the unbiased estimates

$$\frac{\partial \text{Var}(P_u)}{\partial p_i} \quad (2.36)$$

is solved to give the best estimates of the PMF given the data that has been collected. Essentially we are vertically shifting the estimates obtained in each of the histograms in order to minimise the error across the PMF. By convention, we can estimate the error in the PMF by splitting up the statistics collected for the distributions of $P_i^b(\xi)$ and constructing PMFs from these independent samples. For example, we might have collected 100ns of data in each window, but we could construct 5 independent estimates for the PMF using 20ns blocks of trajectories. The Standard Error of the Mean (SEM) can then be used to estimate the error across the surface [14]. By convention, an umbrella sampling calculation is said to have converged when the SEM from these independent samples has fallen below 1kcal/mol across the PMF. Note that there may be sources of systematic error not captured by this criterion.

2.7.2 Metadynamics

Metadynamics has proven to be a popular . The method relies on a time dependent form of U_{bias} given by

$$U_{bias}(\xi, t) = \sum_{\substack{t'=\tau_D, 2\tau_D, \dots \\ t' < t}} B \exp \left(-\frac{(\xi(t) - \xi(t'))^2}{2\sigma^2} \right) \quad (2.37)$$

This means the simulation is dropping virtual, repulsive Gaussian potentials at the positions along ξ in order to encourage the simulation to sample regions of ξ it has not visited already. The process is illustrated in figure ???. The thermodynamic assumption of this method is that the deposition is done slow enough that the system remains at equilibrium, so the Gaussian height B is chosen to be 0.1-0.2 kJ/mol in molecular systems. Usually, the Gaussian widths σ are chosen to be the size of the variance in the unbiased measurements of ξ .

The FES estimate at time t from this method is simply the sum of all the gaussians we have added into the system inverted:

$$U_u(\xi, t) = \frac{1}{t_c - t} \int_{t_c}^t U_b(\xi, t') dt' \quad (2.38)$$

Formally, convergence is reached when the observed probability density is uniform across ξ . That is:

$$P_b(\xi) = \frac{1}{V_\xi} \quad (2.39)$$

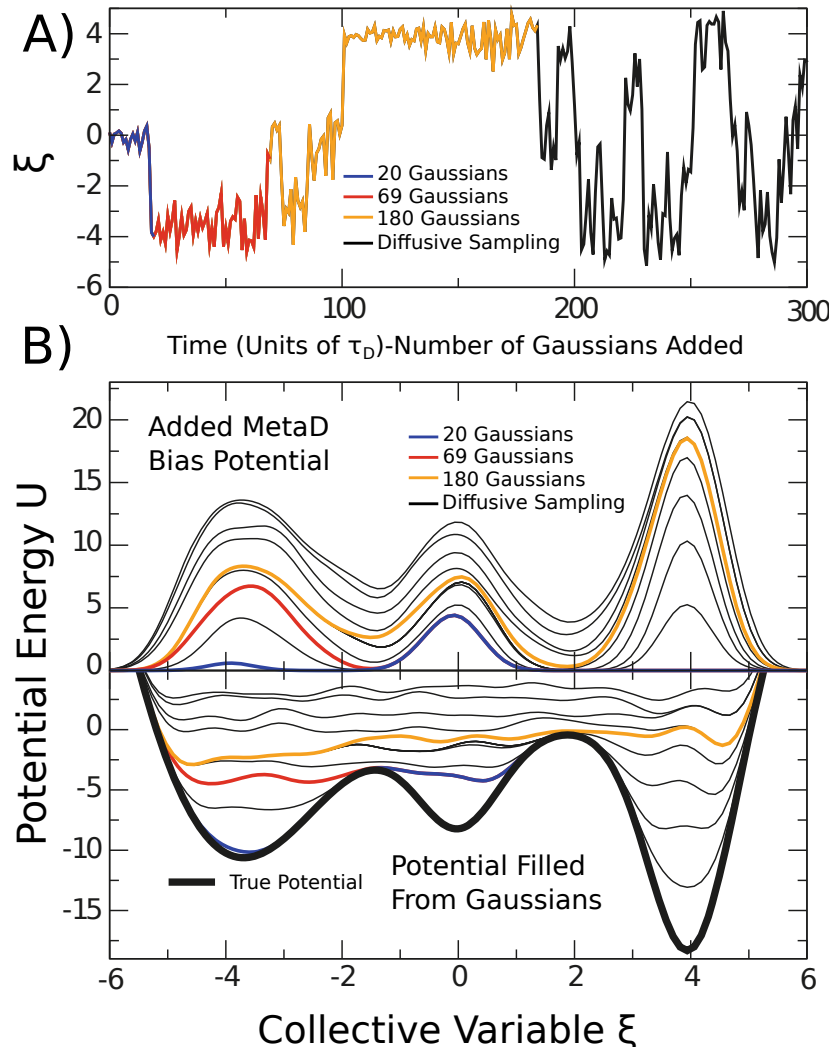


Figure 2.6: Illustration of Metadynamics

A) The trajectory of a collective variable ξ in a metadynamics simulation. The blue region denotes the trajectory up to the time where 20 Gaussians have been deposited. After which the basin at $\xi = 0$ has been filled. The red data points denote the time up until 69 Gaussians have been deposited, after which time the second basin at $\xi = -4$ has been adequately sampled. Finally the Orange data indicates that the 3rd basin at $\xi = 4$ has been adequately sampled after which which time the system begins to sample ξ diffusively and the simulation has converged. B) The upper pannel demonstrates the repulsive potentials that have been added to the simulation in order to drive it to new, unexplored regions. Multiplying the values of this function by -1 will be the estimate of the free energy surface. Note how in the lower panel the true potential the true potential energy surface is gradually filled by the added Gaussians functions. Source[bussi2020]

where V_ξ is the volume of the phase space spanned by ξ . However, conventionally we simply inspect the $U_{bias}(\xi)$ quantity at various intervals for fluctuations about an average function [sun2016].

There are many flavours of metadynamics. The most popular is well-tempered metadynamics which gradually reduces the Gaussian height B as the simulation progresses [barducci2008]. However, this method requires an estimate of how long the simulation will take to converge. There is also infrequent metadynamics which can be used to estimate the diffusion profile along ξ [tiwary2013][tiwary2016][salvalaglio2014].

A useful feature of the Metadynamics method is that it can be linearly sped up with the number of parallel simulations. This is known as multiple walker metadynamics [raiteri2006]. Since we are simply attempting to sample from the same potential U_{MM} up to a desired time, until the criterion in equation 2.39 is met, we can speed this process up by running simulations in parallel and adding Gaussian to the same U_{bias} function.

Conceptually, metadynamics performs the same role as umbrella sampling and should in theory produce the same results in the same system with the same collective variable ξ . However, it has some specific contexts where it outperforms umbrella sampling. This method is more suited to an exploration of free energy space where it can intelligently explore regions which are poorly sampled, whereas umbrella sampling requires some foreknowledge of the surface being investigated. However, metadynamics can be very difficult to converge. A good indicator of such systematic errors are the presence of unphysically large barriers, indicating that there are orthogonal degrees of freedom not sampled along ξ which might correspond to a minimum energy pathway. These barriers will eventually come down in the infinite sampling limit but many barrier crossings will need to be observed.

2.8 Short Comings of Classical MD

The short comings of classical molecular dynamics fall into two classes whose solutions stand opposed to one another. These are the accuracy of the chemical forcefields outlined above and the inability of modern computers to deliver enough samples of the energy landscape to collect sufficient statistics for rigorous conclusions. The issue is that, as the above physical formulation might indicate. The more accurate the forcefields, the more computationally expensive. And so the solutions to the two are constantly in tension with one another. In the next section we will explore the current efforts to bring solutions.

The Problem with Forcefields

These approximations are not without a cost to accuracy. In certain situations, many of which are biologically relevant, it has been shown that quantum effects such as polarisation play an important role in the dynamics of the system. This has been demonstrated in the literature for Gramicidin where polarisable forcefields are able to more accurately reproduce the experimental results of current.

The other context where polarisation is important to consider are on divalent ions.

Here, the solvation energy is underestimated due to the consistent lack of polarisation, making investigations of these biologically important chemical species difficult.

However, for most situations, particularly those involving bulk water and protein motions Molecular Dynamics is proving to be an invaluable tool for investigating the properties of biological systems [hollingsworth2018]. Sadly, it should be kept in mind that classical MD is not able to simulate any chemistry such as forming and breaking or the change a change in profanation state. Such interactions require considerations of Quantum Mechanics which are computationally expensive.

There are several efforts to correct address some of the above issues. These include the inclusion of the effects of polarisation, the most popular methods at the moment being adding a massless drude oscillator as an extra bead to most(?) atoms as in the CHARMM drude forcefields, championed by the Mackerell lab and the use of forcefields such as AMOEBA which explicitly calculate the dipole and quadrupole moments of each atom. These both substantially increase computational cost but have displayed much better agreement with experiments in biological systems where classical forcefields have been shown to fail [35].

Ultimately, the functional form in equation 2.13 used by classical forcefields does not have sufficient degrees of freedom to address all possible chemical contexts. Careful consideration must always be given to whether the forcefield is being used in a faithful way to the situations it was intended to accurately represent. So long as the user is aware of the situations where a given forcefield falls short, classical forcefields can be a powerful tool for the study of molecular systems.

The Problem with Sampling

To physicists the sampling is the more intuitive. Collecting sufficient statistics about the system of interest is difficult and comes at both a computational and human cost. Even though computers have sped up exponentially for the last 50 years we are still orders of magnitude from being able to reach the time scales of many biological processes, as displayed in table ??.

The slow time step demanded in classical MD due to the fast motions of certain atomic groups such as hydrogen is fundamentally at odds with the time scales of many important biological processes such as drug binding or protein folding which occur on the time scale of milliseconds or seconds.

Methods are now emerging which intelligently drive the simulation toward regions unexplored in the collective variable space by unbiased simulations. For some time the field has used steered methods or adaptive sampling methods such as Umbrella Sampling or Metadynamics to drive the simulation toward sections of the energy landscape which are under sampled. These methods universally rely on a choice of collective variable which closely corresponds to a slow degree of freedom. Such a choice is not usually simple. In the case of ion channels one may rationally choose the placement of the ion along the conduction pathway as the collective variable but the choice is less obvious in the case of more global conformational changes.

The success of simulations at the millisecond timescale by D.E Shaw research suggest

that we are in reach of an exciting area in biological research [lindorff-larsen2016]. Enhanced sampling methods will be able to routinely reach motions that occur on these time scales and as software and hardware improve we will be able to push further for larger systems. This indicates that the enhanced sampling approach holds great promise.

The advances we are seeing at the moment which I find exciting are the use of machine learning methods to tease out these degrees of freedom in order to accelerate them with already established free energy methods. These have the potential to uncover new drug binding pockets and revolutionise our understanding of biomolecular systems.

Chapter 3

Review of the Molecular Cause of Cystic Fibrosis

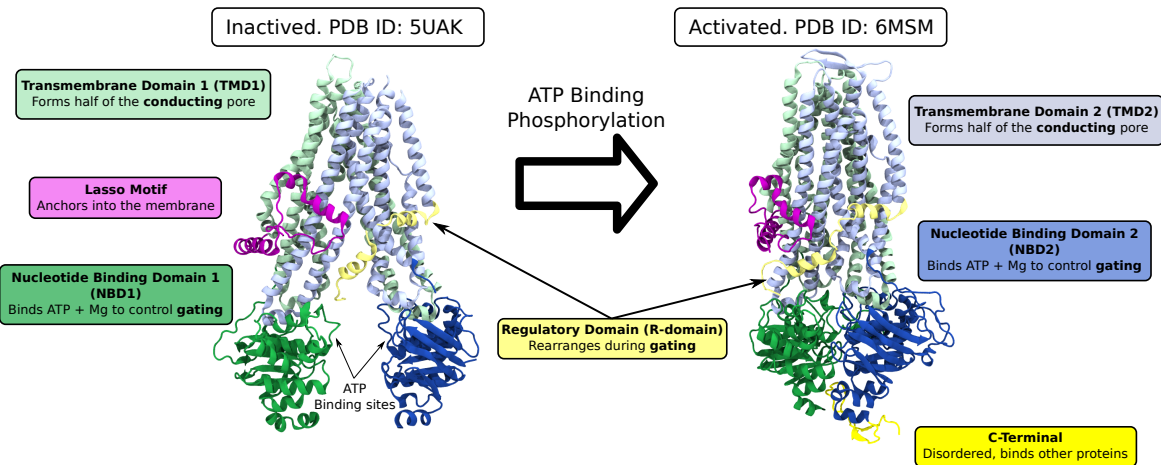


Figure 3.1: CFTR Structure
CFTR's structure and domains

3.1 Clinical outcomes of Cystic Fibrosis

Cystic Fibrosis (CF) is the most common fatal genetic condition in Caucasian populations. 90 000 people are afflicted globally. Even with decades of research there is no known cure for CF. With the average life expectancy of patients falling below 50 even in countries with developed health care systems such as the USA and Australia[54]. The cause is from a build up of salts inside epithelial cells. This causes the surface of the epithelium to dehydrate. When dehydrated the cilia on the epithelium collapse leaving them unable to clear the mucus that naturally lines the airway[55]. The dehydration mentioned earlier causes the mucus to thicken. This buildup has two pathogenic functions. Firstly it inhibits the normal function of the organ, as mucus fills ducts that would normally pass nutrients in the pancreas or absorb gasses in the lungs. Secondly, the stationary mucus allows bacterial infection, this can further degrade lung function and remains one of the most troublesome chronic complications in CF patients.

Much of the clinical research into CF has been managing the movement of this mucus and the populations of bacterium in it. Patients often require hours of physical therapy to help clear this mucus since their lungs are unable to. They must also inhale saline solutions in order to counteract the osmotic pressure in their epithelium. This helps draw more moisture out of the epithelial cells to allow the cilia to move.

CF patients struggle to intake nutrients due to the build up of mucus in their pancreas and large intestines. This leads to CF related diabetes which afflicts roughly half of adults with CF [56]. Patients with CF related diabetes are often administered enzymes and must adhere to a specific diet. A strict diet is particularly important when a patient is taking CFTR modulators because many compounds found in food have interactions with these drugs [57].

3.2 CFTR Structure

CFTR is organised into 7 domains (FIGURE). In the order of their primary sequence they are; The Lasso motif, which anchors into the membrane and serves as an interaction hub with other protein partners such as syntaxin and filamin [1]. Transmembrane Domain 1 (TMD1) which forms half of the pore. Nucleotide Binding Domain 1 (NBD1) which binds ATP when the channel is in the open state. The Regulatory domain (R-domain) which, when phosphorylated allows the channel to open. Transmembrane domain 2 (TMD2) which forms the other half of the ion conducting pore. Nucleotide Binding Domain 2

CFTR belongs to a super family of proteins known as ATP Binding Cassette Transporters, many of these proteins perform active transport across cell membranes. The substrates they transport can vary, including lipids and drug molecules. Proteins in this family share a common motif known as Nucleotide Binding Domains (NBDs). These domains act as ATPases, accelerating the hydrolysis of ATP. The energy from hydrolysis is then transferred into the protein in order for it to pump its substrate against a concentration gradient.

3.3 CFTR classification and structure

The primary cause of the disease Cystic Fibrosis (CF) is the malfunction of a chloride channel, the Cystic Fibrosis Transmembrane Conductance Regulator (CFTR). This ion channel is a member of the ABCC subfamily of ABC transporters, designated ABCC7. This channel is unique amongst this family because it is not generally considered an active transporter but something of a low conductivity channel or a "weak pump" [57].

CFTR is distinguished by a regulatory region known as the R-domain (residues 645-845) which links NBD1 to TMD2. This region acts to lock the channel in the closed state by wedging itself between the TMDs and dislodging when any one of 3 sites are phosphorylated [58]. In experimentally determined structures of human CFTR the secondary structure of a section of the R-domain but not at high enough resolution to determine the identity of individual sidechains [59][60]. Further secondary structure information can be found through experiments with NMR [61].

Previous computational studies of CFTR have been used homology models based on the phosphorylated zebra fish protein PDBID:5W81 [62]. These have yielded interesting results but the sequence similarity between human and zebrafish CFTR is only 55% [1]. For a protein structure where a single amino acid mutation leads to malfunction, more precision can only help. Additionally, the activity of CFTR modulators is not conserved in mutant zCFTR possibly because it has different kinetics to the human channel [1]. In order to do precision medicine we need precision structures.

An open state of the channel has been proposed by combining both the zebra fish homology model and the fully outward facing conformer of a bacterial ABC transporter Sav1866 [63]. Although this model has several characteristics expected of the open channel, such as the critical R352-D993 salt bridge, it lacks a salt bridge between R104-E116. In experiments, these residues could be replaced by cysteines and the

channel would still function. However, when reducing agents were added to the system the channel lost its ability to open fully. This indicates that in the oxidised environment the C104-C116 cysteins formed a disulfide bridge but its breaking upon exposure to reducing agents caused a loss of function in the channel. This indicates that in the WT channel R104-E116 form a stable salt bridge.

This salt bridge is clearly visible in the recent cryo-EM structure of ATP-bound human CFTR [59].

3.4 The Gating Cycle

The conformational transition from inactive to active differs significantly in CFTR compared to other ABC transporters. The NBD domains are largely similar to those found in other ABC transporters, they dimerise in what is termed a head to tail configuration so both subunits contact both bound ATP molecules [] See FIGURE. Residue E1371 allows nucleophilic attack on the γ phosphate of the ATP bound to Walker B [64]. This provides a "kick" to provide the kinetic energy for the opening of the channel CITATION NEEDED.

3.5 Classes of Misfunction to CFTR

The 360 disease causing mutations to CFTR have been classified into 6 common classes based on the nature of the CF they cause, their reaction to CFTR modulators, and results *in vitro* assays. Ultimately I aim to show that at the atomic level these classes of mutations are less meaningful and as patient specific therotyping evolves these classes will become less relevant, serving as illustrative tools only to communicate at a higher level what is going wrong with the CFTR protein. The canonical classification is as follows:

- **Class I** No functional protein. Under these mutations no protein is transcribed due to either problems with the transcription of mRNA or a premature stop codon truncating protein synthesis early, meaning the resulting peptide is missing key domains.
- **Class II** Folding defect. These mutations cause the translated peptide to misfold into the incorrect tertiary structure. This can inhibit the protein's journey as it is trafficked to the cell membrane, its function while once it is there or its functional life time at the surface.
- **Class III** Impaired Gating. Here the mutation inhibits the ability of the protein to transition from the closed to the open state.
- **Class IV** Decreased Conductance. These mutations cause a barrier in the energy landscape of the CFTR chloride conductance pathway.
- **Class V** Less Protein Expressed.
- **Class VI** Decreased Lifetime

Although useful, in reality this paradigm struggles to reflect the fact that a mutation can belong to multiple categories to different levels due to different modes of pathogenesis. Through our molecular simulations we can see that in reality CFTR modulators are capable of treating several different mutations with very different molecular fingerprints.

FIGURE demonstrates how each of the canonical classes at the molecular level is broken down into many sub classes and a mutation might belong to one of many of these subclasses. Structural biology paradigms and *in silico* modelling can help classify mutations into these different classes. In combination with wet lab assays we can understand which classes of these molecular defects are most effectively treated with specific drug regimens. Our computational microscope is helping choose treatments for patients at the atomic level.

3.6 CFTR Modulators

Since CF is caused by malfunctions of the channel it makes sense to pursue CFTR as a drug target. Through high throughput *in vitro* screening several (GET NUMBER) compounds have been developed that aim to rescue the function of CFTR. These fall into two classes. Correctors, which aid CFTR to fold into the correct state and potentiators which help the channel reach the fully open state once it has already folded correctly. Emerging evidence suggests that specific genetic defects may be optimally rescued by specific combinations and doses of both correctors and potentiator compounds. Recently, cryo-EM structures of these compounds in their bound state have been released. In addition to several *in vitro* biophysical experiments to determine the precise mechanism of action and binding site of these compounds.

3.6.1 Correctors

The mechanism of action for corrector compounds appears to be to bind to a pocket between TMH1 and TMH3. Circular dichromism and fluorescence experiments found that an isolated construct of TMH3 and TMH4 were more likely to fold correctly in the presence of corrector compounds. Later cryo-EM structures discovered high resolution electron density in the pocket in the shape of the drug compounds [65].

In combination this is strong evidence for the precise mechanism of action for corrector compounds. Further work will aid in the creation of new compounds to refine our exploitation of this mechanism.

Mention that there are some interactions between correctors and NBD1.

3.6.2 Potentiators

There is more uncertainty surrounding the mechanism of potentiator drugs. Experiments clearly demonstrate that they act directly on CFTR in order to increase the likelihood that it occupies the open state. They bind to the protein with picomolar affinity. There are cryo-EM structures which show the drugs bound to the

TM8 hinge region []. *In vitro* experiments suggest at least two membrane facing binding pockets due to the drugs extreme hydrophobicity[]. The location of this second binding site is unknown. The difficulties arise with mutagenesis experiments. The dose-response curves in several studies show that when various sites are mutated the activity of the drug is lowered. This indicates additional binding sites not yet well defined.

GLPG1837 has not been approved in a clinical setting. *in vitro* experiments suggest that it is more efficacious even though it has lower affinity for CFTR binding (CITATION NEEDED). This would indicate that the highest affinity binding pocket does not produce the greatest modulation. More work is needed to resolve the mechanism which results in the clinical effectiveness of these drugs.

These drugs are clinically efficacious [66] on several mutants with some curious exceptions like N1303K. I suggest the following mechanism for their action. I suspect a similar analogy exists for the action of the correctors. WT-CFTR exhibits a natural landscape with kinetic barriers in the transition between the closed and open states. A gating class mutation to CFTR will introduce a kinetic barrier in the pathway of this conformational transition. What these drugs do is reduce a barrier in the existing conformational landscape of CFTR. This compensates for the barriers introduced by the mutation.

This provides a rationale for why it appears possible for diverse range of molecular defects to be treatable by these small molecules. In our work we've found that the atomic nature of the defects introduced by each mutation varies widely, what is interesting is that experiments in *ex vivo* models have shown that these drugs treat a variety of different defects. The classification of classes of defect is outdated, really there are as many classes as there are mutations.

3.6.3 Annion Selectivity

CFTR is weakly selective for specific anions. F337 is the most important amino acid for selectivity. Bicarbonate (HCO_3^-) is known to have roughly 26% the permeability of chloride through the channel. Note that Fluoride has even higher conductance through CFTR, likely due to its small size and high solvation energy (does this indicate hydrated conductance?). WNK1 is known to influence the selectivity of the channel <https://www.ncbi.nlm.nih.gov/pmc/articles/PMC6889609/>. The permeation of bicarbonate is very important physiologically because if a mutation permeates bicarbonate it means there is a high likelihood the patient will be pancreatic sufficient.

Compared to cation channels like gramicidin and KcsA, CFTR is only weakly selective, permeating a large set of anions with varying radii and geometries. Supposedly it is more permeant to lyotropic (low solvation energy anions) rather than cosmotropic anions (high solvation energy anions) indicating that dehydration of the anion is likely during conductance (CITATION NEEDED). The radius of hydrated chloride ions is 3.2A[67] so even with this larger pore partial dehydration must take place.

3.7 Patient Derived Organoids

The basic unit of living things are cells. In the medical field there is growing capability to discern the functioning of an individual patient's cells. In the field of Cystic Fibrosis Medical Research a recent breakthrough has been to take samples from the epithelium of patients with the disease and grow those samples into tissues which mimic the function of the entire organ[68]. This is possible in the epithelium due to a population of adult stem cells which maintain the ability to differentiate into a variety of cell types (a property known as pluripotency).

Adult stem cells in the epithelium are preferable because other sources of stem cells such as induced pluripotent stem cells (iPSCs) require complex, time consuming protocols to grow into fully developed organoids.

In the case of CF this technology allows the construction of a scalable, patient specific platform where a patient's own tissues can be tested to determine the best treatment for them. These pre-clinical models will allow more patients in the heterogeneous set of disease causing mutations to access modulators.

Forskolin Induced Swelling (FIS) assays have been used to characterise the patient specific response of a patient's organoids to a drug regimen [69].

One limitation of these organoid platforms is the lack of an inflammatory response since no immune cells are present in the tissue culture.

Chapter 4

Concluding Remarks

If this blank in August this is bad.

Bibliography

- (1) Hodgkin, A. L.; Huxley, A. F. *The Journal of Physiology* **1952**, *117*, 500–544, DOI: [10.1113/jphysiol.1952.sp004764](https://doi.org/10.1113/jphysiol.1952.sp004764).
- (2) Braun, E.; Gilmer, J.; Mayes, H. B.; Mobley, D. L.; Monroe, J. I.; Prasad, S.; Zuckerman, D. M. *Living journal of computational molecular science* **2019**, *1*, 5957, DOI: [10.33011/livecoms.1.1.5957](https://doi.org/10.33011/livecoms.1.1.5957).
- (3) Sherrill, C. D., 7.
- (4) *Dynamics of Molecular Collisions: Part B*; Miller, W. H., Ed.; Springer US: Boston, MA, 1976, DOI: [10.1007/978-1-4757-0644-4](https://doi.org/10.1007/978-1-4757-0644-4).
- (5) van Mourik, T.; Bühl, M.; Gaigeot, M.-P. *Philosophical Transactions of the Royal Society A: Mathematical, Physical and Engineering Sciences* **2014**, *372*, 20120488, DOI: [10.1098/rsta.2012.0488](https://doi.org/10.1098/rsta.2012.0488).
- (6) Luo, Z.; Qin, X.; Wan, L.; Hu, W.; Yang, J. *Frontiers in Chemistry* **2020**, *8*.
- (7) Kresse, G.; Furthmüller, J. *Computational Materials Science* **1996**, *6*, 15–50, DOI: [10.1016/0927-0256\(96\)00008-0](https://doi.org/10.1016/0927-0256(96)00008-0).
- (8) Yoo, J.; Aksimentiev, A. *Physical Chemistry Chemical Physics* **2018**, *20*, 8432–8449, DOI: [10.1039/c7cp08185e](https://doi.org/10.1039/c7cp08185e).
- (9) Lemkul, J. A. In *Progress in Molecular Biology and Translational Science*, Strodel, B., Barz, B., Eds.; Computational Approaches for Understanding Dynamical Systems: Protein Folding and Assembly, Vol. 170; Academic Press: 2020, pp 1–71, DOI: [10.1016/bs.pmbts.2019.12.009](https://doi.org/10.1016/bs.pmbts.2019.12.009).
- (10) Chari, S. S. N.; Dasgupta, C.; Maiti, P. K. *Soft Matter* **2019**, *15*, 7275–7285, DOI: [10.1039/C9SM00962K](https://doi.org/10.1039/C9SM00962K).
- (11) Morsali, A.; Goharshadi, E. K.; Ali Mansoori, G.; Abbaspour, M. *Chemical Physics* **2005**, *310*, 11–15, DOI: [10.1016/j.chemphys.2004.09.027](https://doi.org/10.1016/j.chemphys.2004.09.027).
- (12) Phillips, R.; Kondev, J.; Theriot, J.; Garcia, H.; Kondev, J., *Physical Biology of the Cell*, 2nd edition; Garland Science: Boca Raton London New York, 2012.
- (13) Ross, G. A.; Rustenburg, A. S.; Grinaway, P. B.; Fass, J.; Chodera, J. D. *The journal of physical chemistry. B* **2018**, *122*, 5466–5486, DOI: [10.1021/acs.jpcb.7b11734](https://doi.org/10.1021/acs.jpcb.7b11734).
- (14) Gapsys, V.; de Groot, B. L. *eLife* **2020**, *9*, ed. by Faraldo-Gómez, J. D.; Grossfield, A., e57589, DOI: [10.7554/eLife.57589](https://doi.org/10.7554/eLife.57589).

- (15) Klauda, J. B.; Wu, X.; Pastor, R. W.; Brooks, B. R. *The Journal of Physical Chemistry B* **2007**, *111*, 4393–4400, DOI: [10.1021/jp068767m](https://doi.org/10.1021/jp068767m).
- (16) Venable, R. M.; Chen, L. E.; Pastor, R. W. *The Journal of Physical Chemistry B* **2009**, *113*, 5855–5862, DOI: [10.1021/jp900843x](https://doi.org/10.1021/jp900843x).
- (17) Auffinger, P.; Beveridge, D. L. *Chemical Physics Letters* **1995**, *234*, 413–415, DOI: [10.1016/0009-2614\(95\)00065-C](https://doi.org/10.1016/0009-2614(95)00065-C).
- (18) Perera, L.; Essmann, U.; Berkowitz, M. L. *The Journal of Chemical Physics* **1995**, *102*, 450–456, DOI: [10.1063/1.469422](https://doi.org/10.1063/1.469422).
- (19) Roberts, J. E.; Schnitker, J. *The Journal of Chemical Physics* **1994**, *101*, 5024–5031, DOI: [10.1063/1.467425](https://doi.org/10.1063/1.467425).
- (20) Del Buono, G. S.; Figueirido, F. E.; Levy, R. M. *Chemical Physics Letters* **1996**, *263*, 521–529, DOI: [10.1016/S0009-2614\(96\)01234-1](https://doi.org/10.1016/S0009-2614(96)01234-1).
- (21) Essmann, U.; Perera, L.; Berkowitz, M. L.; Darden, T.; Lee, H.; Pedersen, L. G. *The Journal of Chemical Physics* **1995**, *103*, 8577–8593, DOI: [10.1063/1.470117](https://doi.org/10.1063/1.470117).
- (22) Hub, J. S.; de Groot, B. L.; Grubmüller, H.; Groenhof, G. *Journal of Chemical Theory and Computation* **2014**, *10*, 381–390, DOI: [10.1021/ct400626b](https://doi.org/10.1021/ct400626b).
- (23) Darden, T.; York, D.; Pedersen, L. *The Journal of Chemical Physics* **1993**, *98*, 10089–10092, DOI: [10.1063/1.464397](https://doi.org/10.1063/1.464397).
- (24) Hardy, D. J.; Wu, Z.; Phillips, J. C.; Stone, J. E.; Skeel, R. D.; Schulten, K. *Journal of Chemical Theory and Computation* **2015**, *11*, 766–779, DOI: [10.1021/ct5009075](https://doi.org/10.1021/ct5009075).
- (25) Shan, Y.; Klepeis, J. L.; Eastwood, M. P.; Dror, R. O.; Shaw, D. E. *The Journal of Chemical Physics* **2005**, *122*, 054101, DOI: [10.1063/1.1839571](https://doi.org/10.1063/1.1839571).
- (26) Knapp, B.; Ospina, L.; Deane, C. M. *Journal of Chemical Theory and Computation* **2018**, *14*, 6127–6138, DOI: [10.1021/acs.jctc.8b00391](https://doi.org/10.1021/acs.jctc.8b00391).
- (27) Bussi, G.; Donadio, D.; Parrinello, M. *Journal of Chemical Physics* **2007**, *126*, 014101, DOI: [10.1063/1.2408420](https://doi.org/10.1063/1.2408420).
- (28) Martyna, G. J.; Klein, M. L.; Tuckerman, M. *The Journal of Chemical Physics* **1992**, *97*, 2635–2643, DOI: [10.1063/1.463940](https://doi.org/10.1063/1.463940).
- (29) Martyna, G. J.; Tuckerman, M. E.; Tobias, D. J.; Klein, M. L. *Molecular Physics* **1996**, *87*, 1117–1157, DOI: [10.1080/00268979600100761](https://doi.org/10.1080/00268979600100761).
- (30) Karal, M. A. S.; Ahamed, M. K.; Ahmed, M.; Mahbub, Z. B. *RSC Advances* **2021**, *11*, 29598–29619, DOI: [10.1039/D1RA04647K](https://doi.org/10.1039/D1RA04647K).
- (31) Macdonald, A. G. In *Cell Physiology Source Book (Third Edition)*, Sperelakis, N., Ed.; Academic Press: San Diego, 2001, pp 1003–1023, DOI: [10.1016/B978-012656976-6/50151-7](https://doi.org/10.1016/B978-012656976-6/50151-7).
- (32) Allen, M; Tildesley, D, *Computer Simulation of Liquids*; Clarendon Press Oxford: 1991.
- (33) Parrinello, M.; Rahman, A. *Physical Review Letters* **1980**, *45*, 1196–1199, DOI: [10.1103/PhysRevLett.45.1196](https://doi.org/10.1103/PhysRevLett.45.1196).

- (34) Parrinello, M.; Rahman, A. *Journal of Applied Physics* **1981**, *52*, 7182–7190, DOI: [10.1063/1.328693](https://doi.org/10.1063/1.328693).
- (35) Ngo, V.; Li, H.; MacKerell, A. D.; Allen, T. W.; Roux, B.; Noskov, S. *Journal of Chemical Theory and Computation* **2021**, *17*, 1726–1741, DOI: [10.1021/acs.jctc.0c00968](https://doi.org/10.1021/acs.jctc.0c00968).
- (36) Robustelli, P.; Ibanez-de-Opakua, A.; Campbell-Bezat, C.; Giordanetto, F.; Becker, S.; Zweckstetter, M.; Pan, A. C.; Shaw, D. E. *Journal of the American Chemical Society* **2022**, *144*, 2501–2510, DOI: [10.1021/jacs.1c07591](https://doi.org/10.1021/jacs.1c07591).
- (37) Shannon, C. *Proceedings of the IRE* **1949**, *37*, 10–21, DOI: [10.1109/JRPROC.1949.232969](https://doi.org/10.1109/JRPROC.1949.232969).
- (38) Leach, A. R., *Molecular Modelling: Principles and Applications*, 2. ed., 12. [Dr.]; Pearson/Prentice Hall: Harlow, 2009.
- (39) Mazur, A. K. *Journal of Computational Physics* **1997**, *136*, 354–365, DOI: [10.1006/jcph.1997.5740](https://doi.org/10.1006/jcph.1997.5740).
- (40) Feenstra, K. A.; Hess, B.; Berendsen, H. J. *Journal of Computational Chemistry* **1999**, *20*, 786–798, DOI: [10.1002/\(SICI\)1096-987X\(199906\)20:8<786::AID-JCC5>3.0.CO;2-B](https://doi.org/10.1002/(SICI)1096-987X(199906)20:8<786::AID-JCC5>3.0.CO;2-B).
- (41) Andersen, H. C. *Journal of Computational Physics* **1983**, *52*, 24–34, DOI: [10.1016/0021-9991\(83\)90014-1](https://doi.org/10.1016/0021-9991(83)90014-1).
- (42) Hess, B.; Bekker, H.; Berendsen, H. J. C.; Fraaije, J. G. E. M. *Journal of Computational Chemistry* **1997**, *18*, 1463–1472, DOI: [10.1002/\(SICI\)1096-987X\(199709\)18:12<1463::AID-JCC4>3.0.CO;2-H](https://doi.org/10.1002/(SICI)1096-987X(199709)18:12<1463::AID-JCC4>3.0.CO;2-H).
- (43) Balusek, C.; Hwang, H.; Lau, C. H.; Lundquist, K.; Hazel, A.; Pavlova, A.; Lynch, D. L.; Reggio, P. H.; Wang, Y.; Gumbart, J. C. *Journal of chemical theory and computation* **2019**, *15*, 4673–4686, DOI: [10.1021/acs.jctc.9b00160](https://doi.org/10.1021/acs.jctc.9b00160).
- (44) Schlick, T., *Molecular Modeling and Simulation: An Interdisciplinary Guide*, 2nd ed; Interdisciplinary Applied Mathematics v. 21; Springer: New York, 2010.
- (45) Brooks, C. L.; Karplus, M.; Pettitt, B. M., *Proteins: A Theoretical Perspective of Dynamics, Structure, and Thermodynamics*; Advances in Chemical Physics 71; Wiley: New York, 1988.
- (46) Flood, E.; Boiteux, C.; Lev, B.; Vorobyov, I.; Allen, T. W. *Chemical Reviews* **2019**, *119*, 7737–7832, DOI: [10.1021/acs.chemrev.8b00630](https://doi.org/10.1021/acs.chemrev.8b00630).
- (47) Werner, T.; Morris, M. B.; Dastmalchi, S.; Church, W. B. *Advanced Drug Delivery Reviews* **2012**, *64*, 323–343, DOI: [10.1016/j.addr.2011.11.011](https://doi.org/10.1016/j.addr.2011.11.011).
- (48) Meshkin, H.; Zhu, F. *Journal of Chemical Theory and Computation* **2017**, *13*, 2086–2097, DOI: [10.1021/acs.jctc.6b01171](https://doi.org/10.1021/acs.jctc.6b01171).
- (49) Domański, J.; Hedger, G.; Best, R. B.; Stansfeld, P. J.; Sansom, M. S. P. *The Journal of Physical Chemistry B* **2017**, *121*, 3364–3375, DOI: [10.1021/acs.jpca.6b08445](https://doi.org/10.1021/acs.jpca.6b08445).
- (50) Zhu, F.; Hummer, G. *Journal of Chemical Theory and Computation* **2012**, *8*, 3759–3768, DOI: [10.1021/ct2009279](https://doi.org/10.1021/ct2009279).

- (51) Subramanian, N.; Schumann-Gillett, A.; Mark, A. E.; O'Mara, M. L. *Journal of Chemical Information and Modeling* **2019**, *59*, 2287–2298, DOI: [10.1021/acs.jcim.8b00624](https://doi.org/10.1021/acs.jcim.8b00624).
- (52) You, W.; Tang, Z.; Chang, C.-e. A. *Journal of Chemical Theory and Computation* **2019**, *15*, 2433–2443, DOI: [10.1021/acs.jctc.8b01142](https://doi.org/10.1021/acs.jctc.8b01142).
- (53) Zhu, F.; Hummer, G. *Journal of Computational Chemistry* **2012**, *33*, 453–465, DOI: [10.1002/jcc.21989](https://doi.org/10.1002/jcc.21989).
- (54) Kästner, J. *Wiley Interdisciplinary Reviews: Computational Molecular Science* **2011**, *1*, 932–942, DOI: [10.1002/wcms.66](https://doi.org/10.1002/wcms.66).
- (55) Boucher, R. C. Airway Surface Dehydration in Cystic Fibrosis: Pathogenesis and Therapy, 2007, DOI: [10.1146/annurev.med.58.071905.105316](https://doi.org/10.1146/annurev.med.58.071905.105316).
- (56) Kayani, K.; Mohammed, R.; Mohiaddin, H. Cystic Fibrosis-Related Diabetes, 2018, DOI: [10.3389/fendo.2018.00020](https://doi.org/10.3389/fendo.2018.00020).
- (57) Linsdell, P. *Channels* **2018**, *12*, 284–290, DOI: [10.1080/19336950.2018.1502585](https://doi.org/10.1080/19336950.2018.1502585).
- (58) Mihályi, C.; Iordanov, I.; Töröcsik, B.; Csanády, L. *Proceedings of the National Academy of Sciences* **2020**, 202007910, DOI: [10.1073/pnas.2007910117](https://doi.org/10.1073/pnas.2007910117).
- (59) Zhang, Z.; Liu, F.; Chen, J. *Proceedings of the National Academy of Sciences of the United States of America* **2018**, *115*, 12757–12762, DOI: [10.1073/pnas.1815287115](https://doi.org/10.1073/pnas.1815287115).
- (60) Zhang, Z.; Chen, J. *Cell* **2016**, *167*, 1586–1597.e9, DOI: [10.1016/j.cell.2016.11.014](https://doi.org/10.1016/j.cell.2016.11.014).
- (61) Baker, J. M.; Hudson, R. P.; Kanelis, V.; Choy, W. Y.; Thibodeau, P. H.; Thomas, P. J.; Forman-Kay, J. D. *Nature Structural and Molecular Biology* **2007**, *14*, 738–745, DOI: [10.1038/nsmb1278](https://doi.org/10.1038/nsmb1278).
- (62) Zhang, Z.; Liu, F.; Chen, J. *Cell* **2017**, *170*, 483–491.e8, DOI: [10.1016/j.cell.2017.06.041](https://doi.org/10.1016/j.cell.2017.06.041).
- (63) Hoffmann, B.; Elbahnsi, A.; Lehn, P.; Décout, J. L.; Pietrucci, F.; Mornon, J. P.; Callebaut, I. *Cellular and Molecular Life Sciences* **2018**, *75*, 3829–3855, DOI: [10.1007/s0018-018-2835-7](https://doi.org/10.1007/s0018-018-2835-7).
- (64) Stratford, F. L.; Ramjeesingh, M.; Cheung, J. C.; Huan, L. J.; Bear, C. E. *Biochemical Journal* **2007**, *401*, 581–586, DOI: [10.1042/BJ20060968](https://doi.org/10.1042/BJ20060968).
- (65) Fiedorczuk, K.; Chen, J. *Cell* **2022**, *185*, 158–168.e11, DOI: [10.1016/j.cell.2021.12.009](https://doi.org/10.1016/j.cell.2021.12.009).
- (66) Van Goor, F.; Yu, H.; Burton, B.; Hoffman, B. J. *Journal of Cystic Fibrosis* **2014**, *13*, 29–36, DOI: [10.1016/j.jcf.2013.06.008](https://doi.org/10.1016/j.jcf.2013.06.008).
- (67) Yang, K.-L.; Yiakoumi, S.; Tsouris, C. *The Journal of Chemical Physics* **2002**, *117*, 8499–8507, DOI: [10.1063/1.1511726](https://doi.org/10.1063/1.1511726).
- (68) de Poel, E.; Lefferts, J. W.; Beekman, J. M. *Journal of Cystic Fibrosis: Official Journal of the European Cystic Fibrosis Society* **2020**, *19 Suppl 1*, S60–S64, DOI: [10.1016/j.jcf.2019.11.002](https://doi.org/10.1016/j.jcf.2019.11.002).

- (69) Dekkers, J. F. et al. *Nature Medicine* **2013**, *19*, 939–945, DOI: [10.1038/nm.3201](https://doi.org/10.1038/nm.3201).

